Science AAAS

Title: Quantification of Drought During the Collapse of the Classic Maya Civilization

Authors: Nicholas P. Evans[1]*, Thomas K. Bauska[1], Fernando Gázquez[1], Mark Brenner[2], Jason H. Curtis[2], and David A. Hodell[1]

Affiliations:

[1]Godwin Laboratory for Palaeoclimate Research, Department of Earth Sciences, University of Cambridge, Downing Street, Cambridge, CB2 3EQ, United Kingdom.

[2]Department of Geological Sciences, University of Florida, Gainesville, FL 32611, USA.

*Correspondence to: ne243@cam.ac.uk.

Abstract:

The demise of Lowland Classic Maya civilization during the Terminal Classic Period (~800-1000 C.E.) is a well-cited example of how past climate may have impacted ancient societies. Attempts to estimate the magnitude of hydrologic change, however, have met with equivocal success because of the qualitative and indirect nature of available climate proxy data. We reconstructed the past isotopic composition ($\delta^{18}O$, δD, ^{17}O-excess and d-excess) of water in Lake Chichancanab, Mexico, using a novel technique that involves isotopic analysis of the structurally bound water in sedimentary gypsum, which was deposited under drought conditions. The triple oxygen and hydrogen isotope data provide a direct measure of past changes in lake hydrology. We modeled the data and conclude that annual precipitation decreased between 41 and 54%, with intervals of up to 70% rainfall reduction during peak drought conditions, and relative humidity declined by 2 to 7% compared to today.

One Sentence Summary:

We present quantitative estimates of hydro-climate changes that coincided with the demise of the Classic Maya civilization.

Main Text:

More than two decades ago, a sediment core from Lake Chichancanab (Yucatán Peninsula, Mexico; Fig. S1) provided the first physical evidence of a temporal correlation between drought and the sociopolitical transformation of the Classic Maya civilization during the Terminal Classic Period (TCP) (*1*). Presence of gypsum horizons and a concomitant increase in the oxygen isotope ratio ($^{18}O/^{16}O$) in shells of ostracods and gastropods suggested the TCP was among the driest periods of the Holocene in northern Yucatán. Paleoclimate records produced subsequently provided additional evidence for drought during the TCP (*2-9*), but the magnitude of hydro-climate change and its influence on Maya agricultural and sociopolitical systems remains controversial (*10*). The qualitative nature of most climate proxy archives, combined with dating uncertainties, has prevented detailed assessment of the relationship between past climate and cultural changes (*10-12*).

Recent attempts to quantify estimates of past changes in rainfall amount and assess the impact on ancient Maya agriculture have utilized either oxygen ($\delta^{18}O$) (*6, 13*) or hydrogen (δD) (*9-11*) isotopes. No study to date has combined the two isotope systems because materials used for analysis, e.g., carbonates and leaf waxes, preclude simultaneous measurement of the multiple isotopologues of water. Combined analysis of $\delta^{18}O$, $\delta^{17}O$ and δD is a powerful method to estimate past hydrologic changes quantitatively because hydrogen and triple oxygen isotopes each undergo slightly different fractionation during evaporation, leading to changes in the derived d-excess ($\delta D - 8 \cdot \delta^{18}O$) and ^{17}O-excess ($\ln[\delta^{17}O + 1] - 0.528 \ln[\delta^{18}O + 1]$) parameters (*14-19*). In an effectively closed hydrological basin such as Lake Chichancanab, the primary controls on the isotopic fractionation of lake water during evaporation include: the fractional loss of precipitation to evaporation (P/E), normalized relative humidity (RH_n), temperature, and changes in the precipitation source (*1-3, 14*). The d-excess is largely dependent on RH_n and temperature, whereas ^{17}O-excess is controlled mainly by RH_n (*14-19*). Because the predicted trends of d-excess and ^{17}O-excess in evaporating waters display different responses to climate variables, they can be evaluated individually using an iterative model (*20*).

We took advantage of the benefits of using all isotopologues of water and their derived parameters (d-excess and ^{17}O-excess) by measuring triple oxygen and hydrogen isotopes in the hydration water of gypsum ($CaSO_4 \cdot 2H_2O$) in sediment cores from Lake Chichancanab (Fig. S2) (*3*). Today, the lake water is near saturation for gypsum and during past periods of drier climate, when the lake volume shrank, gypsum precipitated from the lake water and was preserved as distinct layers within the accumulating sediments (*1-3*). When gypsum forms, water molecules are incorporated directly into its crystalline structure and this “gypsum hydration water” (GHW) records the isotopic composition of the parent fluid, with known isotopic fractionations (*14, 17, 21-26*). Unlike oxygen isotope fractionation during formation of carbonate minerals (*27, 28*), fractionation during gypsum crystallization is practically independent of temperature (*24*), biological or kinetic (non-equilibrium) effects (*17*). Additionally, isotopes of GHW that are measured in the sedimented gypsum inherently record the driest periods, offering a distinct advantage over other traditional climate archives such as speleothems or mollusk shells, which may fail to register peak drought conditions because of growth hiatuses. Absolute differences in the $\delta^{18}O$, δD, ^{17}O-excess and d-excess, between modern and paleo-lake water, provide an estimate of differences between the lake hydrologic budget during the TCP and today (Fig. 1). Results were evaluated using a numerical isotope mass balance model that must satisfy all isotope variables (*20*) (Fig. S3), and thus provides a more robust constraint on past hydrology than does modeling $\delta^{18}O$ or δD alone.

The modern climate around Lake Chichancanab is characterized by a mean annual precipitation of ~1200 mm, a mean annual surface water temperature of ~26°C and a net annual water deficit of 300-400 mm/yr (*3, 22*). Large changes in precipitation and RH_n occur between the dry (November to May) and rainy seasons (June to October) (*13, 29*). Measured $\delta^{18}O$ and δD of precipitation and groundwater samples from the Yucatán Peninsula, collected from 1994 to 2010, define a local meteoric water line (LMWL) with slope 7.7 (Fig. 2). Evaporation enriches the lake in the heavier water isotopes (2.6‰ < $\delta^{18}O$ < 3.8‰ and 10.1‰ < δD < 17.2‰), evolving along an evaporative line defined by $\delta D = 5.1 \cdot \delta^{18}O - 3.1$. This evaporation line intersects the LMWL at $\delta^{18}O$ = -4.7(±1.2)‰ and δD = -27.5(±10.7)‰, which is within error of the mean oxygen and hydrogen isotope values recorded in local rivers and groundwater from regional IAEA GNIP stations ($\delta^{18}O$ = -4.1‰; δD = -24.3‰) (*29*) and this study ($\delta^{18}O$ = -4.0‰; δD = -23.5‰).

The gypsum deposited during the droughts of the Terminal Classic and early Postclassic Periods was used to calculate the $\delta^{18}O$, $\delta^{17}O$ and δD of the paleo-lake water, which ranged from 3.6‰ to 4.9‰ for $\delta^{18}O$, 1.9‰ to 2.5‰ for $\delta^{17}O$, and 13.7‰ to 18.8‰ for δD (Fig. 1). Mean values of the paleo-lake waters ($\delta^{18}O$ = 4.2‰; $\delta^{17}O$ = 2.2‰; δD = 16.4‰) during drought episodes are enriched in the heavier isotopes compared to modern lake values ($\delta^{18}O$ = 3.1‰; $\delta^{17}O$ = 1.6 ‰; δD = 12.7‰). Age uncertainty associated with the lake record and periods of gypsum precipitation was calculated using Bayesian age-depth analysis of radiocarbon ages obtained from the sediment cores (*3*) (Fig. 1). The probabilities of drought occurring specifically during the onset (~750 to ~850 C.E) and the end (~950 to ~1050 C.E.) of the TCP are high ($P > 0.85$ and $P > 0.95$, respectively) (*20*). Multiple proxy climate records across the Maya Lowlands also provide evidence of drought synchronicity, with only slight temporal variations across the region (*10*).

To estimate quantitatively the magnitude of drought during the TCP, we employed a transient model that explicitly simulates the evolution of the isotopic and chemical composition of the lake water, including the gypsum flux to the lake sediments (Fig. S3). The modeled gypsum flux can be compared to observed variations in the gypsum content of the sediments, as expressed by variations in sediment bulk density (*3*). Changes in lake surface-area-to-volume ratio were obtained from the lake bathymetry (Fig. S4). The model was run at sub-monthly resolution in a series of millennial-duration experiments, forced with North American Regional Reanalysis (NARR) data for local precipitation and RH_n. We first tested the model using the climate forcing across the modern sampling period from 1994 to 2010 (Fig. S5). It successfully reproduced the mean of modern isotope data, with insignificant gypsum precipitation. This time interval, which was fortuitously one of the driest of recent decades, was then used as the baseline for comparison to paleo-simulations.

To provide scenarios that are directly comparable to the GHW data, we performed long transient simulations in which rainfall and RH_n were reduced by variable amounts to simulate a series of multi-decadal-scale droughts. The use of a model allows us to compare, directly and quantitatively, climate conditions that affect the modern lake, with those of plausible drought conditions. First, only the intervals over which the model produced gypsum deposition (modeled sediment density >1.1 g/cm^3) were selected. The periods of modeled gypsum accumulation were then aggregated into drought conditions for a given scenario via two pathways: (i) all model variables were averaged across all of the droughts, and (ii) probability density functions were constructed incorporating the variability within and between each decadal-length drought. Data consistent scenarios were then selected by excluding those model runs that fell outside the 1σ range of the isotope data and where, on average, the model failed to produce significant gypsum accumulation (cutoff of average density <1.2 g/cm^3 based on 1σ range; Fig. S6). Two possible scenarios were tested subsequently: (i) a reduction in precipitation with accompanying shifts in the isotopic composition of rainwater (i.e. the amount effect) and, (ii) a reduction in precipitation with accompanying decreases in RH_n (Fig. 3).

In the first scenario, precipitation $\delta^{18}O$ was reduced with an increase in rainfall according to the amount effect relationship (i.e., $\delta^{18}O_{precipitation}/\Delta Precipitation_{volume} = -0.0121‰/mm$; Fig. S7) with associated changes in δD and $\delta^{17}O$ that track the Global MWL (i.e., no changes in d-excess or ^{17}O-excess). No scenarios with these assumptions are able to reproduce the relationship between $\delta^{18}O$, d-excess and ^{17}O-excess observed in the data. If the constraints provided by d-excess and ^{17}O-excess are removed and only $\delta^{18}O$ and gypsum precipitation are employed, our model permits reductions in precipitation that average 50% over all drought intervals (Fig. 3, blue lines). This estimate is in broad agreement with previous work that relied on carbonate $\delta^{18}O$-derived precipitation estimates (using the local amount effect), which predicted reductions of up to 40% (*6, 13*). Our greater estimate of 50% is in part a consequence of the peak drought $\delta^{18}O$ values recorded by gypsum, as well as the integration of simulated gypsum formation and true lake bathymetry in the model. Crucially, however, the added information from the d-excess and ^{17}O-excess data suggests that multi-decadal shifts in the $\delta^{18}O$ of precipitation (caused by the amount effect) were not the dominant factor that affected the isotope budget of Lake Chichancanab during the TCP.

In the second scenario, we reduced precipitation without changes in the $\delta^{18}O$ of precipitation, but instead with concurrent changes in RH_n. In this case we observed excellent agreement between the modeled evolution of all isotopic data, with increases in $\delta^{18}O$ accompanied by decreases in d-excess and ^{17}O-excess (Fig. 3, red lines). This analysis yielded plausible scenarios of precipitation reduction that average 47% across all droughts (with a 1σ level of 41-54%) accompanied by RH_n reductions of 4% (1σ level 2-7%). This result provides a robust, quantitative estimate of the mean annual hydrological conditions of the combined drought periods during the TCP at Lake Chichancanab.

Although the time evolution of our model is not a direct reconstruction of climate conditions, the model permits heterogeneity within and between each decade-long drought. The ±1σ range determined from the probability density functions indicates that the precipitation reduction could vary from 20 to 70% throughout the modeled droughts (Fig. 3). This variability represents the transition into and out of drought phases and demonstrates that the severity of the droughts could be intense (up to a 70% reduction in precipitation), while maintaining the isotope balance and without desiccating the lake. Although variability in the seasonal delivery of rainfall (or lack thereof) is difficult to constrain because the residence time of the lake water is greater than an annual cycle, our results provide quantitative estimates for the total annual reduction in the water available for agriculture and domestic use for the ancient Maya. Importantly, recorded Colonial-period accounts of later droughts, e.g., 1535-1560 and 1765-1773, during which high mortality, famines, and population displacement were reported (*30*), are not manifest as intervals of gypsum precipitation in Lake Chichancanab. The lack of gypsum formation is likely a result of shorter duration and/or lower severity of these droughts, providing further evidence that the TCP was an unusually dry period for the Holocene on the Yucatán Peninsula.

Using triple oxygen and hydrogen isotope data to independently deconvolve climate variables precipitation, RH_n and the amount effect, we constrained the changing hydrological conditions at Lake Chichancanab. This approach provides a significant advance over previous attempts to estimate the magnitude of rainfall reduction during the TCP droughts (e.g. *6, 13*). Furthermore, these quantitative estimates of past rainfall and RH_n can serve as input variables in crop models, to better understand how drought affected agriculture (e.g., maize production) in the northern Maya Lowlands during the TCP (*12*).

References:

[1] D. A. Hodell, J. H. Curtis, M. Brenner. Possible role of climate in the collapse of Classic Maya civilization. *Nature* **375** (6530), 391-394 (1995).

[2] D. A. Hodell, M. Brenner, J. H. Curtis, T. Guilderson. Solar forcing of drought frequency in the Maya lowlands. *Science* **292** (5520), 1367-1370 (2001).

[3] D. A. Hodell, M. Brenner, J. H. Curtis. Terminal Classic drought in the northern Maya lowlands inferred from multiple sediment cores in Lake Chichancanab (Mexico). *Quat. Sci. Rev*. **24** (12), 1413-1427 (2005).

[4] J. H Curtis, D. A. Hodell, M. Brenner. Climate variability on the Yucatán Peninsula (Mexico) during the past 3500 years, and implications for Maya cultural evolution. *Quat. Res*. **46** (1), 37–47 (1996).

[5] G. H. Haug, D. Günther, L. C. Peterson, D. M. Sigman, K. A. Hughen, B. Aeschlimann. Climate and the collapse of Maya civilization. *Science* **299**, 1731–35 (2003).

[6] M. Medina-Elizalde S. J. Burns, D. W. Lea, Y. Asmerom, L. von Gunten, V. Polyak, M. Vuille, A. Karmalkar. High resolution stalagmite climate record from the Yucatán Peninsula spanning the Maya Terminal Classic period. *Earth Planet. Sci. Lett.* **298** (1), 255-262 (2010).

[7] D. J. Kennett, S. F. Breitenbach, V. V. Aquino, Y. Asmerom, J. Awe, J. U. Baldini, P. Bartlein, B. J. Culleton, C. Ebert, C. Jazwa, M. J. Macri. Development and disintegration of Maya political systems in response to climate change. *Science* **338**, 788–791 (2012).

[8] D. Wahl, F. Estrada-Belli, L. A. Anderson. 3,400 year paleolimnological record of prehispanic human–environment interactions in the Holmul region of the southern Maya lowlands. *Palaeogeogr. Palaeoclimatol. Palaeoecol*. **379–380**, 17–31 (2013).

[9] P. M. Douglas, M. Pagani, M. A. Canuto, M. Brenner, D. A. Hodell, T. I Eglinton, J. H. Curtis. Drought, agricultural adaptation, and sociopolitical collapse in the Maya lowlands. *Proc. Natl. Acad. Sci*. **112** (18), 5607-5612 (2015).

[10] P. M. Douglas, A. A. Demarest, M. Brenner, M. A. Canuto. Impacts of climate change on the collapse of lowland Maya civilization. *Annu. Rev. Earth Planet. Sci.* **44**, 613-645 (2016).

[11] P. M. Douglas, M. Brenner, J. H. Curtis. Methods and future directions for paleoclimatology in the Maya lowlands. *Glob. Planet. Change* **138**, 3-24 (2016).

[12] J. Yaeger, D. A. Hodell. *Climate-culture-environment interactions and the collapse of Classic Maya civilization*. In: D. H. Sandweiss and J. Quilter (Eds.), *El Nino, Catastrophism, and Culture Change in Ancient America*, Dumbarton Oaks, pp. 187-242 (2008).

[13] M. Medina-Elizalde, E. J. Rohling. Collapse of Classic Maya civilization related to modest reduction in precipitation. *Science* **335** (6071), 956-959 (2012).

[14] F. Gázquez, M. Morellón, T. K. Bauska, D. Herwartz, J. Surma, A. Moreno, M. Staubwasser, B. Valero-Garcés, A. Delgado-Huertas, D. A. Hodell. Triple oxygen and hydrogen isotopes of gypsum hydration water for quantitative paleo-humidity reconstruction. *Earth Planet. Sci. Letts.* **481**, 177-188 (2018).

[15] H. Craig, L. I. Gordon. Deuterium and oxygen 18 variations in the ocean and the marine atmosphere. Pp. 9–130. In E. Tongiorgi (ed.),.*Stable isotopes in oceanographic studies and paleotemperatures*. Consiglio nazionale delle ricerche, Laboratorio di geologia nucleare, Pisa (1965).

[16] J. R. Gat. Oxygen and hydrogen isotopes in the hydrologic cycle. *Annu. Rev. Earth Planet. Sci.* **24**, 225–262 (1996).

[17] D. Herwartz, J. Surma, C. Voigt, S. Assonov, M. Staubwasser. Triple oxygen isotope systematics of structurally bonded water in gypsum. Geo*chim. Cosmochim. Acta* **209**, 254–266 (2017).

[18] B. Luz, E. Barkan. Variations of $^{17}O/^{16}O$ and $^{18}O/^{16}O$ in meteoric waters. *Geochim. Cosmochim. Acta* **74**, 6276–6286 (2010).

[19] J. Surma, S. Assonov, M. J. Bolourchi, M. Staubwasser. Triple oxygen isotope signatures in evaporated water bodies from the Sistan Oasis, Iran. *Geophys. Res. Lett.* **42**, 8456–8462 (2015).

[20] Materials and methods are available as supporting material on *Science* Online.

[21] Z. Sofer. Isotopic composition of hydration water in gypsum. *Geochim. Cosmochim. Acta* **42**, 1141–1149 (1978).

[22] D. A. Hodell, A. V. Turchyn, C. J. Wiseman, J. Escobar, J. H. Curtis, M. Brenner, A. Gilli, A. D. Mueller, F. Anselmetti, D. Ariztegui, E. T. Brown. Late Glacial temperature and precipitation changes in the lowland Neotropics by tandem measurement of $\delta^{18}O$ in biogenic carbonate and gypsum hydration water. *Geochim. Cosmochim. Acta* **77**, 352–368 (2012).

[23] N. P. Evans, A. V. Turchyn, F. Gázquez, T. R. Bontognali, H. J. Chapman, D. A. Hodell. Coupled measurements of $\delta^{18}O$ and δD of hydration water and salinity of fluid inclusions in gypsum from the Messinian Yesares member, Sorbas Basin (SE Spain). *Earth Planet. Sci. Lett.* **430**, 499–510 (2015).

[24] F. Gázquez, N. P. Evans, D. A. Hodell. Precise and accurate isotope fractionation factors ($\alpha^{17}O$, $\alpha^{18}O$ and αD) for water and $CaSO_4 \cdot 2H_2O$ (gypsum). *Geochim. Cosmochim. Acta* **198**, 259–270 (2017).

[25] F. Gázquez, J. M. Calaforra, N. P. Evans, D. A. Hodell. Using stable isotopes ($\delta^{17}O$, $\delta^{18}O$ and δD) of gypsum hydration water to ascertain the role of water condensation in the formation of subaerial gypsum speleothems. *Chem. Geol.* **452**, 34-46 (2017).

[26] F. Gázquez, I. Mather, J. Rolfe, N. P. Evans, D. Herwartz, M. Staubwasser, D. A. Hodell. Simultaneous analysis of $^{17}O/^{16}O$, $^{18}O/^{16}O$ and $^{2}H/^{1}H$ of gypsum hydration water by cavity ring-down laser spectroscopy. *Rapid Commun. Mass Spectrom.* **29**(21), 1997-2006 (2015).

[27] T. Kluge, H. P. Affek. Quantifying kinetic fractionation in Bunker Cave speleothems using Δ47. *Quat. Sci. Rev.* **49**, 82–94 (2012).

[28] M. S. Lachniet. Climatic and environmental controls on speleothem oxygen-isotope values. *Quat. Sci. Rev.* **28**(5), 412–432 (2009).

[29] L. I. Wassenaar, S. L. Van Wilgenburg, K. Larson, K. A. Hobson. A groundwater isoscape (δD, $\delta^{18}O$) for Mexico. *J. Geochem. Explor.* **102**, 123–136 (2009).

[30] J. A. Hoggarth, M. Restall, J. W. Wood, D. J. Kennett. Drought and its demographic effects in the Maya lowlands. *Current Anthropology*, **58**(1), 82–113 (2017).

Figures:

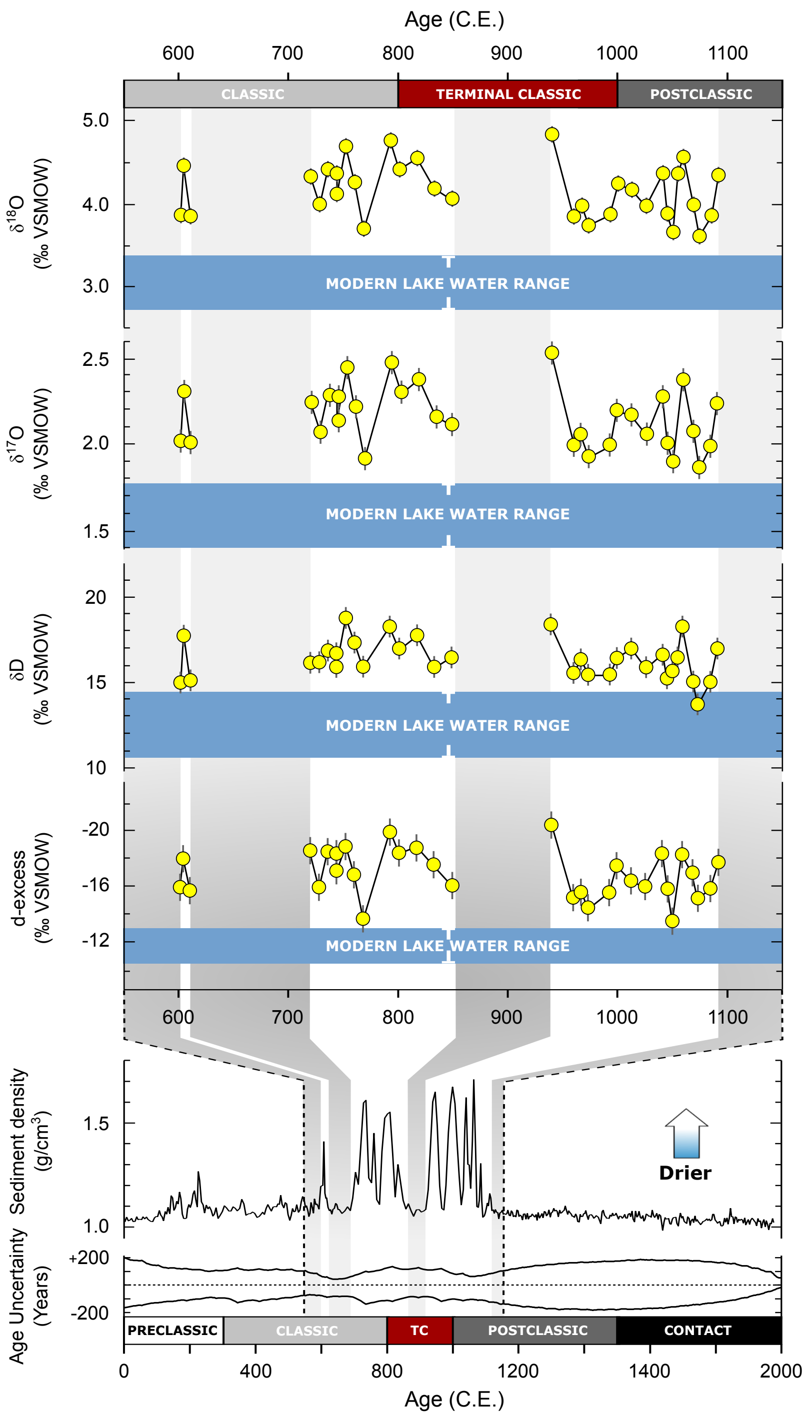

Fig. 1: Water isotopes during drought periods compared to modern water isotopes of Lake Chichancanab. (**Lower**) Sediment density record of core CH1 7-III-04 from 0 to 2000 C.E. (shown relative to Maya chronology) (*3*). Periods of gypsum precipitation are indicated by density values >1.1 g/cm^3. Age uncertainty (95% confidence intervals) are derived from Bayesian age-depth analysis and normalized to

the best-fit age model (*20)* (Fig. S8). (**Upper**) $\delta^{18}O$, $\delta^{17}O$, δD and d-excess (δD – 8 · $\delta^{18}O$) of paleo-lake water data (yellow circles) from 550 to 1150 C.E shown after correction of measured GHW for known fractionation factors (*24*) at 26°C. Horizontal blue band defines the mean (±1σ) isotopic composition recorded in the modern lake. Positive $\delta^{18}O$, $\delta^{17}O$ and δD values and negative d-excess values reflect periods of drought. Note d-excess axis is reversed. Abbreviation: VSMOW, Vienna Standard Mean Ocean Water.

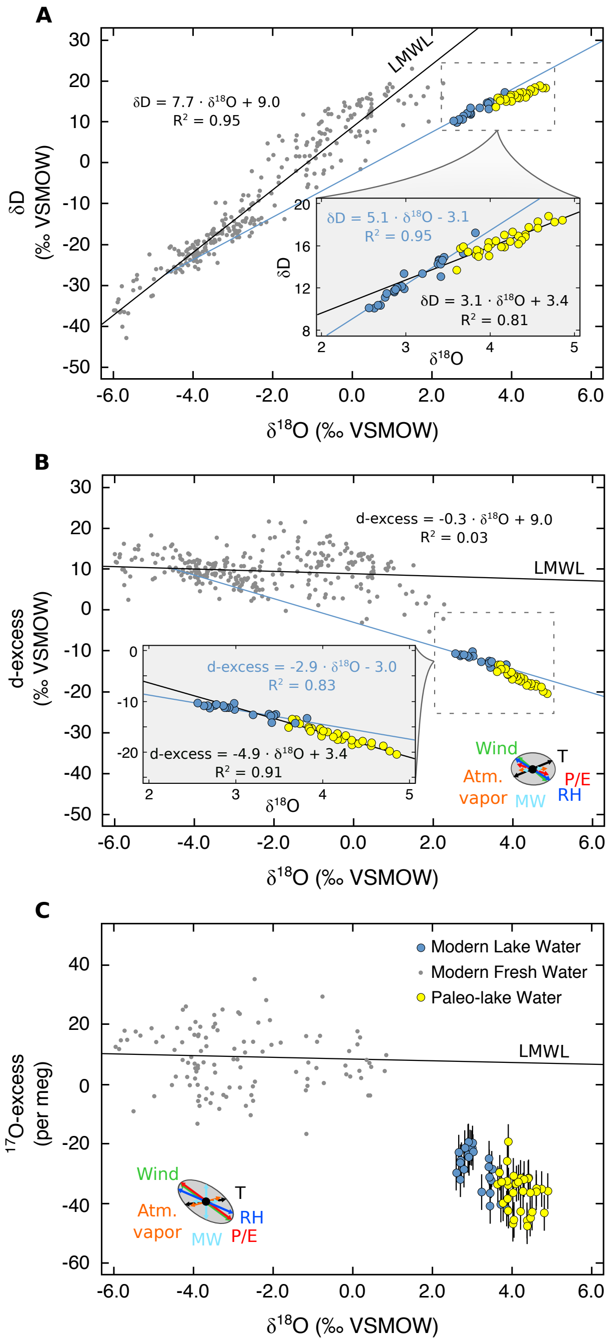

Fig. 2: Comparison of measured local meteoric water (gray circles), modern lake water (blue circles) and paleo-lake water data (yellow circles). Paleo-lake water data are shown after correction of measured GHW for known fractionation factors (*24*) at 26°C. In (**A**) $\delta^{18}O$ vs δD, (**B**) $\delta^{18}O$ vs d-excess (d-excess = $\delta D - 8 \cdot \delta^{18}O$) and (**C**) $\delta^{18}O$ vs ^{17}O-excess (^{17}O-excess = $\ln[\delta^{17}O + 1] - 0.528\ \ln[\delta^{18}O + 1]$) space, local meteoric water measurements define the local meteoric water line (LMWL). Paleo-lake water in **A**, **B** and **C** displays greater enrichment along an evaporative trend

compared to modern lake waters. The grey ellipses define relative influence of variables that can affect the isotopic composition of water in $\delta^{18}O$ vs d-excess and $\delta^{18}O$ vs ^{17}O-excess space; Precipitation/Evaporation (P/E), normalized relative humidity (RH_n), temperature (T), changes to source composition (MW), the degree of equilibrium between atmospheric vapor and fresh water (Atm. vapor), and turbulence created by wind (Wind) (*14*). The size of each arrow is derived from the tolerance given for each input parameter in Table S8.

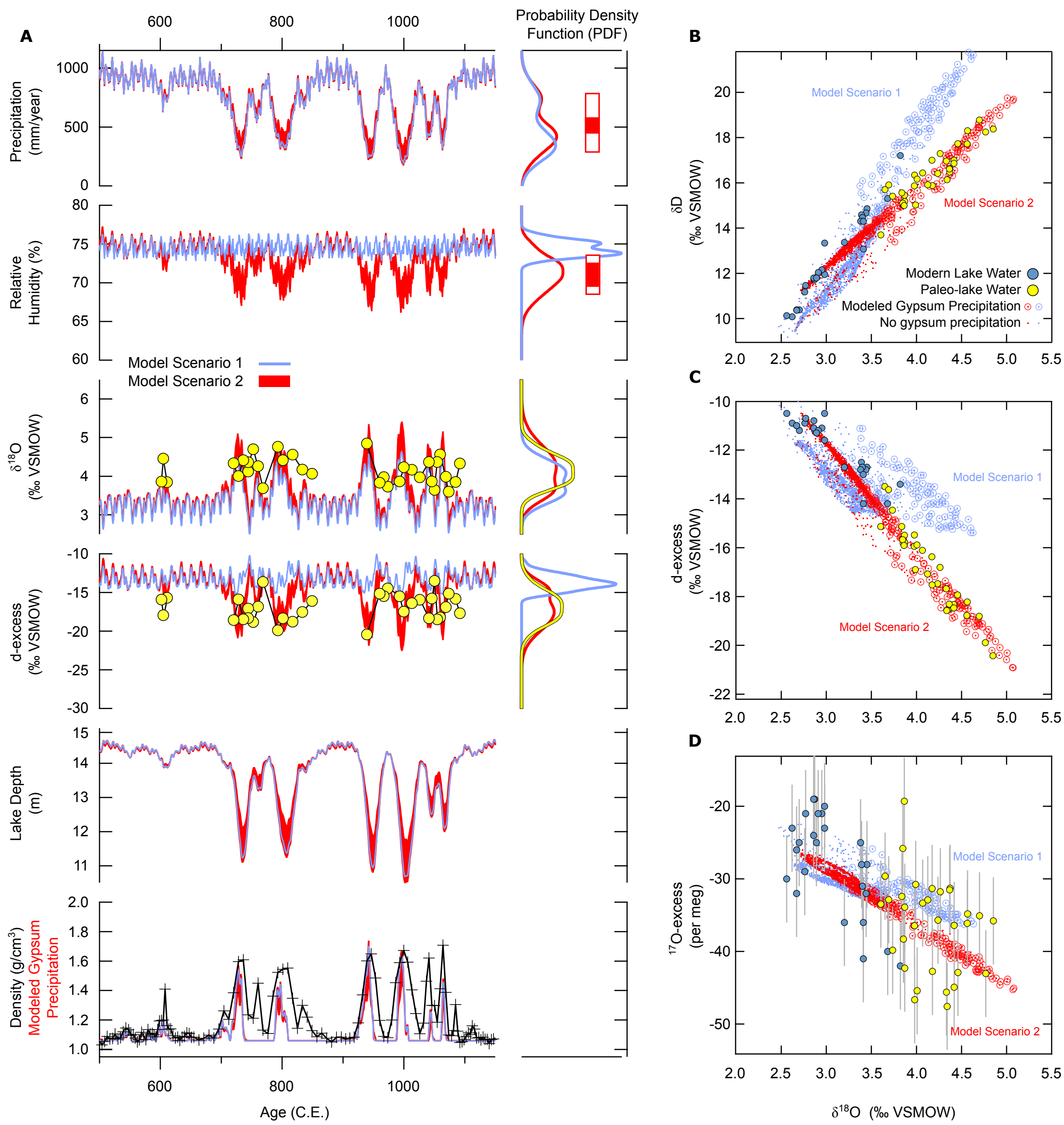

Fig. 3: (**A**) Transient model of the lake system from 550 to 1200 C.E. GHW data (yellow circles) and core density are plotted against sampling ages derived from Bayesian age-depth analysis (*20*). Multi-decadal-scale droughts were simulated by forcing (1) a reduction in precipitation with accompanied shifts in the isotopic composition of rainwater (i.e., the amount effect: $\delta^{18}O_{precipitation}/\Delta Precipitation_{volume}$ = –0.0121‰/mm; Scenario 1, blue line) and (2) reductions in precipitation with accompanied decreases in RH_n (Scenario 2, red field). Probability density functions incorporate the variability within and between each decade-long drought (GHW data = yellow line; scenario 1 = blue line; scenario 2 = red line). Scenario 1 fails to match

the d-excess data derived from GHW. Scenario 2 successfully reproduces all $\delta^{18}O$ and d-excess data. When all model variables were averaged across all droughts, the mean precipitation and RH_n reduction (closed red boxes adjacent to PDFs) is 47% (with a 1σ level of 41-54%) and 4% (1σ level 2-7%), respectively. The ±1σ range determined from probability density functions (open red boxes adjacent to PDFs) shows the variability of precipitation and RH_n throughout the droughts. Scenarios 1 and 2 are also plotted as (**B**) $\delta^{18}O$ vs δD, (**C**) $\delta^{18}O$ vs d-excess and (**D**) $\delta^{18}O$ vs ^{17}O-excess. Open circles indicate points in the model at which gypsum is precipitating; dots indicate modeled data points when gypsum is not precipitating. Error bars (±1σ) are shown or are smaller than the symbols.

Acknowledgments:

We thank James Rolfe for technical assistance and support with stable isotope measurements, and three anonymous reviewers for insightful comments that improved the paper. **Funding**: The research leading to these results received funding from the European Research Council under the European Union's Seventh Framework Program (FP/2007-2013)/ERC grant agreement n. 339694 (Water Isotopes of Hydrated Minerals) to D.A.H. **Author Contributions**: D.A.H., N.P.E. and F.G. developed the analytical method and designed the study. M.B., J.H.C., and D.A.H. collected the original sediment cores from Lake Chichancanab. N.P.E. sampled the cores, and N.P.E. and F.G. performed all isotopic analyses. T.K.B. designed the transient model and performed drought simulations. N.P.E., T.K.B. and D.A.H. wrote the paper with contributions from all other authors. **Competing Interests**: The authors declare no competing interests. **Data Availability**: All data are available in the manuscript or supplementary material, and at www.ncdc.noaa.gov/paleo/study/24476.

Supporting Online Material:

Materials and Methods

Modeling

Table S1 – S10

Fig S1 – S11

References (31 – 54)

Science
AAAS

Supplementary Materials for

Quantification of Drought During the Collapse of the Classic Maya Civilization

Nicholas P. Evans*, Thomas K. Bauska, Fernando Gázquez, Mark Brenner, Jason H. Curtis, and David A. Hodell.

correspondence to: ne243@cam.ac.uk

This PDF file includes:

1.0 Materials and Methods:

1.1 Sediment Cores and Sampling:

Lake Chichancanab is located at ~19°51'21"N 88°45'49"W, Yucatán Peninsula, SE Mexico (Fig. S1). In March 2004, core CH1 7-III-04 was collected from Lake Chichancanab with a piston corer in 14.7 m of water (*3*). Shortly after collection, cores were split, wrapped in plastic film and stored at 4°C. Core sections were measured for bulk density by gamma-ray attenuation by Hodell et al. (*3*), and contain high-density gypsum bands interbedded with low-density organic layers (Fig. S2). Gypsum was sampled at 0.5 cm intervals – individual crystals were picked from the >350 μm size fraction and ground to a powder. Powdered samples were dried in an oven at 45°C for 15-20 hours and placed under vacuum (~10^{-3} mbar) for ~3 hours to remove adsorbed water prior to hydration water extraction (*31*).

1.2 Gypsum Hydration Water (GHW):

GHW was extracted from each sample (150-200 mg) by heating to 400°C and trapping the evolved water, *in vacuo*, using a bespoke offline extraction system described in Gázquez et al. (*26*). Triple oxygen (^{16}O, ^{17}O, ^{18}O) and hydrogen (H, D) isotopes of the GHW were measured by cavity ring down spectroscopy (CRDS) in the Godwin Laboratory, University of Cambridge, UK (Table S1), using an L2140-i Picarro CRDS water isotope analyzer with an attached micro-combustion module (MCM; Picarro Inc.) (*26, 32*). The MCM's cartridge was filled with a pyrolytic catalyst to remove any organic contaminants in the GHW that may spectroscopically interfere with the CRDS analyses (*26*). Triple oxygen and hydrogen isotope results are reported in parts per thousand (‰) relative to V-SMOW. External error (1σ) was estimated by repeated analysis (n = 11) of an analytical-grade standard extracted along with the samples (*26*). Internal standards were calibrated previously against V-SMOW, GISP, and SLAP for $\delta^{18}O$ and δD, and against V-SMOW and SLAP for $\delta^{17}O$-$\delta^{18}O$ (*33*). 1σ was ±0.07‰ for $\delta^{17}O$, ±0.12‰ for $\delta^{18}O$, ±0.63‰ for δD, ±0.8‰ for d-excess and ±6 per meg (±0.006‰) for ^{17}O-excess (Table S2).

d-excess and ^{17}O-excess are defined as:

$$\text{d-excess} = \delta D - 8 \cdot \delta^{18}O$$
$$^{17}O\text{-excess} = \ln(\delta^{17}O + 1) - 0.528 \ln(\delta^{18}O + 1)$$

Where 0.528 is the slope of the modern $\delta^{17}O$ - $\delta^{18}O$ Global MWL (*34)*.

Whereas study of GHW in lakes has produced relevant paleoclimatic records that agree closely with other local and regional climate proxies (*14, 22-24, 35, 36*), GHW can undergo post-depositional isotopic exchange under certain conditions (e.g. temperature fluctuations >60°C during sediment burial and exhumation cycles) (*37, 38*). We suggest the gypsum in Lake Chichancanb preserves the isotopic composition of the lake water at the time of deposition and has not undergone post-depositional diagenesis or exchange with modern lake water. After applying fractionation factors, the isotopic values of the paleo-lake waters are considerably enriched compared to the modern lake (Fig. 1; Fig. S2). If the GHW had exchanged with sediment pore water, a relatively homogeneous isotopic profile, with values similar to the current lake water, would be expected. What is more, the burial depth of the gypsum is shallow (< 2 m) and the sediments are porous, thus isotopic gradients in pore water would be strongly attenuated by diffusion and advection with overlying lake water (*14*).

1.3 Precipitation, meteoric and lake water samples:

We report the triple oxygen and hydrogen isotopic measurement of lake water (n = 156), river and ground water (n = 92), and rainwater (n = 31) samples from stations across the Yucatán Peninsula, collected from 1994 to 2010 (Fig. S10; Tables S3, S4 and S5). Measurements were made using an L2140-i Picarro CRDS water isotope analyzer. The majority of rainwater samples were collected at 20°00'59"N 89°01'13"W, ~30 km west of Lake Chichancanab (*22*). All water samples were collected and stored in Qorpak bottles with Polyseal cone-lined caps to prevent evaporation.

1.4 Biogenic carbonate measurements:

Shells and shell fragments of the gastropod *Pyrgophorus coronatus* were picked from 0.5 cm intervals of core CHI 7-III-04. Shells were cracked and sonicated in methanol to remove contaminant debris. Subsequently, samples were treated with 10% H_2O_2 for 30 minutes to remove organic matter, dried and ground to a fine powder. Stable oxygen isotopes of carbonate were measured using a ThermoScientific GasBench II, equipped with a CTC autosampler coupled to a MAT253 mass spectrometer (*39*). Samples were flushed with CP grade helium then acidified with 104% H_3PO_4 and reacted at 70°C for 1 hour. Repeat analysis of the Carrara Marble standard yielded a 1σ analytical precision of ±0.1‰ for $\delta^{18}O$. Results are reported relative to the Vienna Pee Dee Belemnite (VPDB). Small sample fragments were run on a Kiel III carbonate preparation device interfaced with a Finnigan MAT 252 mass spectrometer. Analytical precision was estimated at ±0.08‰ for $\delta^{18}O$.

1.5 Code:

All code can be found in the supplementary file "Evans_et_al_2018_Matlab_Model" on *Science* Online. Please address enquiries to T.K.B. (tkb28@cam.ac.uk).

2.0 Modeling:

2.1.1 Transient Model Details:

The transient box model presented here is a lake basin with a surface and deep box (Fig. S4A). The volume (4.57e7 m^3), surface area (1.02e7 m^2), and surface area to depth relationship conform to data presented in Hodell et al. (*3*) (Fig. S4B). This geometry equates to a mean depth of 4.5 m in the model with the modern deepest area of the basin equal to ~15 m.

The basin is fed by a precipitation flux determined by NARR reanalysis data (~1 m water equivalent/m^2/a; Fig. S5) with a constant catchment size through time. The basin hydrology is effectively closed (*40*). Groundwater flux to and from the lake (equivalent to ~10% of precipitation) delivers Ca^{2+}, SO_4^-, Na^{2+}, K^+, Mg^{2+} and Cl^- and maintains the lake near the modern salt balance, with gypsum near saturation. Water is lost via evaporation, which is held constant at a rate of 1.07 m water equivalent/m^2/a with the absolute flux evolving through time, depending on the surface area of the lake.

The saturation state of gypsum was calculated offline with the PHREEQC model for a wide range of solutions, starting at modern conditions. The lake model incorporates these solutions in a look-up table to calculate the gypsum saturation at every time step. If the lake exceeds saturation, Ca^{2+} and SO_4^- is removed by gypsum precipitation at a rate that maintains the lake below saturation, with a response time of 1 year. Combining the mass of gypsum precipitated and surface area of the lake at a given time-step allows us to calculate the gypsum accumulation in the lake sediment. This is then used to calculate a synthetic core log of density, assuming the density of accumulating gypsum is 2.31 g/cm^3 and that the accumulation of other sediments is constant at 0.941 mm/year, with a density of 1.06 g/cm^3 based on the mean sediment accumulation that brackets the drought periods.

2.1.2 Transient Model Isotope and Ionic Mass Balance:

The isotope mass balance model employs a Craig-Gordon evaporation scheme (*15*) as formulated in Criss (*41*). The overall isotopic fractionation during evaporation (α_{evp}) depends on the equilibrium fractionation (α_{eq}), kinetic fractionation (α_{kin}), relative humidity (h) and the isotopic ratio of water vapor (R_v) and the evaporating surface of the basin (R_b), whereby:

$$\alpha_{evp} = \alpha_{eq}\alpha_{kin}\left(\frac{1-h}{1-\alpha_{eq}h\frac{R_v}{R_b}}\right) \quad (1)$$

Equilibrium fractionation (α_{eq}) for H_2O^{18} ($\alpha^{18}O_{eq}$) and DHO (αD_{eq}) are calculated using an assumed lake surface temperature of 25°C and the equations of Horita and Wesolowski (*42*). The equilibrium fractionation for H_2O^{17} is then a function $\alpha^{18}O_{eq}$, where:

$$\alpha^{17}O_{eq} = \alpha^{18}{O_{eq}}^{\theta eq}$$

and θ_{eq} is 0.529 (*43*).

Kinetic fractionation factors for all three minor isotopes are calculated as a function of wind-induced turbulence (w), lake surface temperature (T) and the kinetic fractionation parameter between ^{18}O and ^{17}O (θ_{kin}):

$$\alpha^{18}O_{kin} = 1.0283^{w}$$
$$\alpha D_{kin} = (1.25 - 0.02T)(\alpha^{18}O_{kin} - 1) + 1$$
$$\alpha^{17}O_{kin} = \alpha^{18}{O_{kin}}^{\theta kin}$$

We assume R_v depends on the degree to which the atmospheric water vapor (v_{eq}) is in equilibrium with R_p (*44*) where:

$$R_v = R_p(\alpha_{eq(p-v)} V_{eq})$$

The general form of the mass-balance equation for the mass of a given species (mX) of either isotope or ion in basin box 1 (b1) is:

$$\frac{dmX_{b1}}{dt} = F_P R_P - F_{evp} R_{evp} + F_{gb1} R_g - F_{b1g} R_{b1} + F_{b2b1} R_{b2} - F_{b1b2} R_{b1}$$

Similarly the mass balance for basin box 2 (b2) is:

$$\frac{dmX_{b2}}{dt} = F_{b1b2}R_{b1} - F_{b2b1}R_{b2}$$

In this set of equations F represents the various fluxes of water in terms of mass of the major water isotope (HHO^{16}) and R represents the ratio of minor isotope or ionic species relative to HHO^{16}. As examples, the ratio of deuterium in box 1 is:

$$R_{DHO,b1} = \frac{mDHO_{b1}}{mHHO^{16}{}_{b1}}$$

The concentration of Ca in box 1 is:

$$R_{[Ca],b1} = \frac{mCa_{b1}}{mHHO^{16}{}_{b1}}$$

When the overall water mass balance is calculated (i.e. the variation in volume):

$$R_{HHO^{16},b1} = 1$$

Ratios for external isotopic such as the precipitation and groundwater fluxes are referenced relative to VSMOW such that:

$$R_{DHO,p} = \left(\frac{\delta D_p}{10^3} + 1\right) R_{DHO,VSMOW}$$

The isotopic ratios of the evaporation flux (R_{evp}) are determined from Equation 1 and the isotopic ratios of the basin surface (R_{b1}):

$$R_{evp} = \frac{R_{b1}}{\alpha_{evp}}$$

2.1.3 Transient Model Parameterization:

When modeling the isotopic composition of the paleo-lake, the (1) lake surface temperature (T), (2) wind-induced turbulence (w), (3) isotopic composition of the atmospheric vapor, (4) salinity effect on isotope fractionation, and (5) the isotopic composition of the freshwater input (and any variability caused by the amount effect) must be known or assumed (Table S6).

1. To constrain water temperature changes at Lake Chichancanab during the Terminal Classic Period (TCP), tandem measurements of both gypsum hydration water (GHW) and carbonate $\delta^{18}O$ that were deposited concurrently permit the deconvolution of the $\delta^{18}O$ carbonate signal into its temperature and $\delta^{18}O$-water components via the carbonate paleo-temperature equation (*22*). To calculate the temperature at which the aragonitic shells of *Pyrgophorus coronatus* formed, we used the equation of Grossman and Ku (*45*) that is based on analysis of foraminifera (*Hoeglundina elegans*) and gastropods:

$$T\ °C = 21.8 - 4.59(\delta^{18}O_{arag\ PDB} - \delta^{18}O_{water\ SMOW})$$

The $\delta^{18}O$ of gastropod aragonite and GHW is used to estimate $\delta^{18}O_{arag}$ and $\delta^{18}O_{water}$, respectively. Gypsum and gastropod samples were only used if they were in direct contact with each other, or the shell fragments were found embedded within gypsum. The derived temperature from *Pyrgophorus coronatus* and gypsum from the same bed averaged 25.9±1.7°C (Table S7). This temperature is indistinguishable from the mean annual temperature of the lake today (*22*). Equally, because ^{17}O-excess is minimally affected by temperature changes, moderate variations in mean temperature result in insignificant effects on the trajectories of the evaporated waters. For example, 5°C of temperature change has a small effect on the model results for ^{17}O-excess (up to ~±2 per meg in a terminal lake), whereas d-excess changes by as much as ~3‰ in a terminal lake, when all other parameters remain constant (*14*). Thus, the model sensitivity to temperature changes is low.

2. It is known that the proportion of $\alpha^{18}O_{kin}$ may be suppressed by turbulent flow induced by wind (*46*), and therefore wind could alter isotope mass balance, especially for d-excess and ^{17}O-excess. The exponent 'w' is set between 0.5 (pure turbulence) and 1 (no wind). Measured wind speeds in the region of Lake Chichancanab are ~3 m/s and relatively constant over the year (*47*), resulting in a well-mixed lake-surface layer. When turbulence is not considered, the model yields d-excess and ^{17}O-excess values that are systematically too low compared to the analytical data for some modern periods. We also tested this variable by analyzing modern and paleo-lake water data using previously published Monte Carlo models (*14*) (Section 2.1.5). These tests provide the best fit to modeled data when w is kept constant at ~0.5 when modeling both the modern and the TCP GHW data.

3. The isotopic composition of modern atmospheric vapor is not well constrained in the Yucatán Peninsula, nor are there estimates available for how this variable has changed in the past. Assuming equilibrium with local meteoric water, the isotopic composition of atmospheric water vapor can be approximated (*14*). Gibson et al. (*44*), however, suggested that the isotopic composition of atmospheric vapor is often only in partial equilibrium with that of local freshwater. We assumed a degree of equilibrium of 60%, a reasonable estimate for most tropical and inter-tropical regions (*44*). Note that Gázquez et al. (*14*) show that the triple oxygen and hydrogen system is relatively sensitive to the isotopic composition of the vapor, especially for coastal lakes affected by advection of marine vapor masses. In coastal lakes, the isotopic composition of the modern atmospheric vapor is in equilibrium with seawater rather than freshwater. This is probably not the case at Lake Chichancanab, which is located ~140 km inland.

4. High concentrations of NaCl and other salts within a lake can cause the water isotopic activity ratios to diverge from the corresponding concentration ratios, as a consequence of isotopic fractionation between free water and water in

ionic hydration shells (*17, 48*). This “salt effect” is different for hydrogen and oxygen isotope fractionation, resulting in complications when interpreting the relationship between $\delta^{18}O$ and δD at salt concentrations >100,000 mg/L (*17, 48*). The total dissolved salt concentration in Lake Chichancanab today is ~4000 mg/L (*3*). Substantial oxygen and hydrogen isotope fractionation effects caused by high salinity would not be expected at these low concentrations (*41, 48*). During periods of lake drawdown, the transient model displays elevated salt concentrations, but concentrations that approach 100,000 mg/L are never experienced in model runs.

5. The mean (±1σ) modern isotopic composition of regional groundwater is -4.0 ± 1.7‰ for $\delta^{18}O$, -2.10 ± 0.9‰ for $\delta^{17}O$ and -23.5 ± 12.8‰ for δD. We used $\delta^{18}O$ = -4.5‰ and δD = -26‰ (so that d-excess = 10‰) and set ^{17}O-excess = 2.5 per meg to model present-day conditions. These variables were held constant throughout the transient model runs, although they can be systematically varied to reflect isotope effects such as the amount effect (see below and Section 2.1.4). We tested the effect of non-systematic variability on the isotopic composition of meteoric water (using bounds of ±0.5‰ for $\delta^{18}O$, ±5‰ for d-excess, and ±9.5 per meg for ^{17}O-excess), using the steady state Monte Carlo model of Gázquez et al. (*14*) to quantify derived uncertainty (Section 2.1.5).

The amount effect (i.e. correlation between depletion of heavy isotopes in rainfall with greater amount of rain) is thought to play a role in the Yucatán Peninsula and thus the isotopic composition of meteoric water may vary over the timescales modeled (*6, 13*). The amount effect and its perturbation in the $\delta^{18}O$ of precipitation (P) over a seasonal cycle was calculated from isotopic composition of precipitation collected at 20°00'59"N 89°01'13"W (*22*), and rainfall amounts from the proximal meteorological station at Dziuche, 19°54'00"N 88°48'40"W, from 2006 to 2009. The linear regression ($\delta^{18}O$ = -0.0176(P) - 0.1204; R^2 = 0.92) is very similar to that found by Medina-Elizalde et al. (*6*) from the IAEA station in Veracruz, México ($\delta^{18}O$ = -

0.0118(P) - 0.64; R^2 = 0.80). We compiled data from Veracruz between 1969 and 1985 (omitting years with poor data coverage) and the records from Chichancanab between 2006 and 2009 (*22*). The compiled linear regression for $\delta^{18}O$ ($\delta^{18}O$ = -0.0121(P) - 0.41) displays a significant correlation (R^2 = 0.73), whereas there was no significant amount effect displayed by d-excess or ^{17}O-excess (Fig. S7).

2.1.4 Deconvolution of climatic variables:

$\delta^{18}O$, ^{17}O-excess and d-excess are affected to differing degrees by changes in RH_n, the ratio P/E, temperature, turbulence (e.g., wind) on the water surface during evaporation, the isotopic composition of the atmospheric water vapor, changes to the isotopic composition of the input source (*14, 19, 41, 44*). In $\delta^{18}O$-^{17}O-excess and $\delta^{18}O$-d-excess space, the predicted trends of waters undergoing evaporation (in partial equilibrium with atmospheric vapor) show that ^{17}O-excess and d-excess are largely sensitive to RH_n and the ratio P/E, moderately sensitive to the isotopic composition of freshwater input, turbulence on the water surface during evaporation and to the isotopic composition of the atmospheric water vapor, whereas their sensitivities to temperature are relatively small, especially for ^{17}O-excess (Fig. 2) (*14*). Because the isotopic composition of the freshwater input, along with variance in the turbulence on the water surface during evaporation, the isotopic composition of the atmospheric water vapor, and temperature are relatively well constrained (Section 2.1.3; Table S6), variability in RH_n, P/E and changes in the isotopic composition of the freshwater input (caused by the amount effect) can be deconvolved in model scenarios.

To provide semi-realistic scenarios that are directly comparable to the GHW data, transient simulations were run in which NARR precipitation and RH_n forcings were reduced by variable amounts to simulate a series of multi-decadal-scale droughts (Fig. 3; Fig. S3). Precipitation and/or RH_n forcings are directly modulated by the density record of core CH1-III-04 (*3*); the maximum variability during a run was set to the maximum density point over time, and precipitation and/or RH_n were reduced linearly across all months. Absolute reductions in P/E and RH_n were referenced relative to mean NARR data over the period from 1994 to 2010. In other words, a 50% reduction in precipitation and a 5% reduction in RH_n would equate to 50% less rainfall in each month (e.g. 200mm/mth to 100mm/mth), and a decrease in the absolute RH_n by 5 percentage units each month (e.g. RH_n = 75% to RH_n = 70%) during a modeled time period compared to the 1994 to 2010 baseline.

During model runs, the intervals of modeled gypsum accumulation were first selected from a pre-determined density range (modeled sediment density >1.1 g/cm^3). The periods of modeled gypsum accumulation were then aggregated into drought conditions for a given scenario in two ways: (i) all model variables were averaged across all the droughts, and (ii) probability density functions were constructed incorporating the variability within and between each decadal-length drought (Fig. S3). To identify the timing of significant gypsum accumulation, we selected periods of modeled sediment density >1.2 g/cm^3. This would be equivalent to selecting data outside one standard deviation of the mean sediment density from core CH1-III-04 (1.09±0.11 g/cm^3), calculated from the total sediment density record of Hodell et al. (*3*) from 500 B.C. to 2000 C.E. (Fig. S6A). Modeled data from these periods were then compared to mean (±1σ) GHW data. The model runs were selected as positive when the modeled δ^{18}O, d-excess and ^{17}O-excess (during periods of significant gypsum precipitation) fell within one standard deviation (1σ) of the GHW data (Fig. S6). A major constraint on the modeled P/E variability is the sediment density range from which the modeled data are selected. As displayed in Fig. S6, if the modeled sediment density threshold is changed from 1.2 g/cm^3, the lower bound of P/E and RH_n estimates will vary systematically. Importantly, increasingly conservative estimates for periods of gypsum precipitation (i.e. modeled sediment density >1.2 g/cm^3) produce increasingly more severe reductions in baseline P/E and RH_n.

Two scenarios were tested: (i) a reduction in precipitation with accompanying shifts in the isotopic composition of rainwater (i.e. the amount effect) and, (ii) a reduction in precipitation with accompanying decreases in RH_n. In scenario 1 (main text; Fig. 3), the density record modulates changes in the P/E ratio. Modeled precipitation δ^{18}O was simultaneously varied according to the amount effect relationship (i.e. $\delta^{18}O_{precipitation}/\Delta Precipitation_{volume} = -0.0121‰/mm$; Fig. S7). As the associated changes in δD and $\delta^{17}O$ track the Global MWL, no changes in d-excess or ^{17}O-excess are imposed in these scenarios. No scenarios were able reproduce the relationship between $\delta^{18}O$, d-excess and ^{17}O-excess observed in the data. In scenario 2, changes in the ratio P/E were coupled with changes to RH_n.

It should also be noted that a combination of RH_n reduction and the amount effect could potentially reproduce the observed data during the TCP. Although a combination of RH_n reduction and (a suppressed) amount effect cannot be definitively ruled out, given the great number of possible outcomes when modeling three variable parameters, our experiments show that the amount effect does not dominate the isotopic budget of the lake. Thus, any influence of the amount effect (in combination with RH_n reductions) at Lake Chichancanab during the TCP will have little effect on modeled outcomes because of the dominance of RH_n in the ^{17}O-excess and d-excess signal.

2.1.5 Monte Carlo Modeling Scenarios:

In addition to transient model experiments described above and in the main body of the text, we also used a previously described steady state model of the lake in a series of Monte Carlo experiments to determine the range of climatological conditions that simultaneously satisfy all stable isotope results of GHW, in combination with statistical estimates of uncertainty (Fig. S9) (*14*). In these scenarios, the parameter "Xe" represents the hydrologic balance of the lake. A scenario in which all water is lost by outflow and no evaporation occurs is represented as Xe = 0, whereas a scenario in which all water is lost to evaporation (i.e. a terminal basin) is represented as Xe = 1. The Xe of Lake Chichancanab is not believed to have changed over the last ~1500 years and near-terminal conditions are thought to have prevailed (*40*). Equally, Gázquez et al. (*14*) show that when Xe ranges from 0.75 to 1, changes in this parameter barely affect the RH_n values derived from this Monte Carlo model. Here, we chose conservative estimates of Xe between 0.8 and 0.9 to cover all likely variability (Table S8).

Modeled GHW data suggest there was a reduction in RH_n of between 2 and 9% during the TCP, compared to the period when modern lake water was sampled (1994-2010), in good agreement with our transient experiments (2-7%) (Table S9). Estimated errors for RH_n are smaller than 4% (1σ) when all variables listed in Table S8 are considered. The slightly greater estimates for reductions in RH_n relative to the transient model arise because the steady-state assumption in the Monte Carlo model precludes an accurate simulation of isotopic balance during lake level fluctuations. Because the model does not account for the additional isotopic enrichment in the lake due to decreased P/E during a lake-level drawdown, it is slightly biased towards higher estimates of RH_n reduction.

2.2 Age Models:

Radiocarbon ages for core CH1 7-III-04 were obtained by Hodell et al. (*3*). We estimated calendar ages with 95% confidence intervals using the Bayesian Age-Depth Modeling software "BACON" in R (Fig. S8) (*49*). Derived age-depth error (95% confidence intervals) was normalized to the best-fit line to produce age-depth errors for the Chichancanab density record (*3*) (Fig. 1; Table S10). To quantify age uncertainty in relation to the timing of dry intervals, we inverted the density record of core CH1-III-04 and identified data outside one standard deviation of the mean sediment density from core CH1-III-04. This would be equivalent to selecting sediment densities >1.2 g/cm^3, equivalent to the periods from which GHW was extracted. The BACON function 'Events' was then used to quantify the probability of arid conditions at any calendar age. Fifty-year window widths were used, with the windows moving at 10-year steps from the core's bottom ages to its top (Fig. S11) (*49*).

We also used Bayesian age modeling techniques to synthesize the regional proxy records of Curtis et al. (*4*), Wahl et al. (*8*) and Douglas et al. (*50*) (Fig. S11). To quantify age uncertainty in relation to the timing of dry intervals, we inverted the records and identified the lowest 10th percentile of the raw data for Wahl et al. (*8*) and Douglas et al. (*50*), and the 5-point smooth of the $\delta^{18}O$ *Cytheridella ilosvayi* record from Curtis et al. (*4*).

All proxy records dated using radiometric techniques yielded a significant age uncertainty. Overall, although individual records show subtle variations in drought timing, the age uncertainty results in the chance of drought occurring any time between 500 and 1300 C.E. (*51*). Gypsum deposition at Lake Chichancanab displays a significant chance of occurring from ~750 to ~850 C.E (Probability of drought at 800 C.E. = 0.85), coinciding with the onset of the collapse of Terminal Classic Maya Civilization (Fig. S11).

Supplementary Tables:

Table S1:

Isotopic composition of measured gypsum hydration water (GHW) and calculated lake mother water (MW) from samples recovered from core CH1 7-III-04, Lake Chichancanab. Asterisk denotes samples that were analyzed with the MCM of the L2140-i Picarro CRDS turned off; $\delta^{17}O$ results were considered unreliable (*26*) and samples were not used in modeling analysis.

Sample name	Age (A.D.)	$\delta^{17}O$ (GHW)	$\delta^{18}O$ (GHW)	δD (GHW)	$\delta^{17}O$ (MW)	$\delta^{18}O$ (MW)	δD (MW)	^{17}O-excess (MW)	d-excess (MW)
A									
CHI 07-III-04 128.0-128.5 cm	1092	4.08	7.81	-2.66	2.24	4.33	17.0	-46	-17.7
CHI 07-III-04 129.0-129.5 cm	1085	3.83	7.33	-4.58	1.99	3.85	15.0	-38	-15.8
CHI 07-III-04 130.5-131.0 cm	1073	3.70	7.08	-5.86	1.87	3.60	13.7	-33	-15.1
CHI 07-III-04 130.5-131.0 cm*	1073		6.95	-5.69		3.48	13.9		-14.0
CHI 07-III-04 131.0-131.5 cm	1069	3.91	7.46	-4.57	2.07	3.99	15.0	-31	-16.9
CHI 07-III-04 132.0-132.5 cm	1059	4.21	8.04	-1.35	2.37	4.57	18.3	-35	-18.2
CHI 07-III-04 132.5-133.0 cm*	1055		7.84	-3.14		4.37	16.5		-18.5
CHI 07-III-04 133.0-133.5 cm	1050	3.73	7.12	-3.90	1.90	3.65	15.7	-30	-13.5
CHI 07-III-04 133.5-134.0 cm	1046	3.84	7.34	-4.41	2.01	3.87	15.2	-34	-15.8
CHI 07-III-04 133.5-134.0 cm	1046		7.20	-4.42		3.72	15.2		-14.6
CHI 07-III-04 134.0-134.5 cm	1041	4.11	7.85	-2.99	2.27	4.37	16.6	-31	-18.3
CHI 07-III-04 134.0-134.5 cm*	1041		7.58	-3.29		4.10	16.3		-16.5
CHI 07-III-04 135.5-136.0 cm	1026	3.90	7.45	-3.74	2.06	3.98	15.9	-36	-15.9
CHI 07-III-04 136.0-136.5 cm	1013	4.01	7.65	-2.63	2.17	4.17	17.0	-31	-16.4
CHI 07-III-04 136.5-137.0 cm	1000	4.04	7.71	-3.20	2.20	4.24	16.4	-36	-17.5
CHI 07-III-04 137.0-137.5 cm	993	3.83	7.34	-4.14	2.00	3.87	15.5	-42	-15.5
CHI 07-III-04 139.5-140.0 cm	973	3.77	7.21	-4.19	1.93	3.73	15.4	-40	-14.5
CHI 07-III-04 139.5-140.0 cm*	973		7.55	-2.21		4.07	17.4		-15.1
CHI 07-III-04 140.0-140.5 cm	967	3.89	7.45	-3.27	2.05	3.98	16.3	-47	-15.5
CHI 07-III-04 140.5-142.5 cm*	960		7.47	-3.50		3.99	16.1		-15.8
CHI 07-III-04 140.5-141.5 cm	960	3.83	7.31	-4.04	1.99	3.84	15.6	-32	-15.1
CHI 07-III-04 142.0-142.5 cm	939	4.36	8.33	-1.27	2.52	4.85	18.4	-36	-20.4
CHI 07-III-04 142.0-142.5 cm*	939		8.14	-1.50		4.66	18.2		-19.2
B									
CHI 07-III-04 148.0-148.5 cm	849	3.95	7.54	-3.18	2.11	4.07	16.4	-33	-16.1
CHI 07-III-04 148.5-149.0 cm*	841		7.71	-3.50		4.24	16.1		-17.8
CHI 07-III-04 149.0-149.5 cm	833	4.00	7.65	-3.72	2.16	4.18	15.9	-43	-17.5
CHI 07-III-04 150.0-151.0 cm	817	4.21	8.04	-1.92	2.37	4.56	17.7	-36	-18.8
CHI 07-III-04 151.0-151.5 cm	801	4.13	7.89	-2.62	2.29	4.42	17.0	-36	-18.3
CHI 07-III-04 151.5-152.0 cm	793	4.31	8.24	-1.40	2.47	4.77	18.2	-43	-19.9
CHI 07-III-04 153.0-153.5 cm	768	3.75	7.17	-3.70	1.91	3.69	15.9	-33	-13.6
CHI 07-III-04 153.0-153.5 cm*	768		7.54	-2.40		4.07	17.2		-15.3
CHI 07-III-04 153.5-154.0 cm	760	4.05	7.74	-2.34	2.22	4.26	17.3	-32	-16.8
CHI 07-III-04 154.0-154.5 cm	752	4.28	8.18	-0.88	2.44	4.70	18.8	-35	-18.8
CHI 07-III-04 154.0-154.5 cm*	752		8.25	0.43		4.77	20.1		-18.1
CHI 07-III-04 154.5-155.0 cm	744	3.98	7.60	-3.69	2.14	4.12	15.9	-33	-17.1
CHI 07-III-04 154.5-155.0 cm	744	4.11	7.84	-3.01	2.27	4.37	16.6	-32	-18.3
CHI 07-III-04 155.0-155.5 cm	736	4.12	7.89	-2.76	2.28	4.42	16.9	-45	-18.5
CHI 07-III-04 155.5-156.0 cm	728	3.90	7.48	-3.44	2.07	4.01	16.2	-45	-15.9
CHI 07-III-04 156.0-156.5 cm	720	4.08	7.81	-3.47	2.24	4.34	16.1	-48	-18.6
C									
CHI 07-III-04 166.0-166.5 cm	611	3.84	7.32	-4.48	2.00	3.85	15.1	-26	-15.7
CHI 07-III-04 167.0-167.5 cm	605	4.15	7.93	-1.91	2.31	4.46	17.7	-43	-17.9
CHI 07-III-04 167.5-168.0 cm	602	3.86	7.34	-4.59	2.02	3.86	15.0	-19	-15.9

Table S2:

External and internal reproducibility of GHW measurements.

EXTERNAL PRECISION	$\delta^{17}O$	$\delta^{18}O$	δD	^{17}O-excess	d-excess
NEWGYP L6 27/8/15	0.21	0.37	-49.78	12	-52.3
NEWGYP L6 9/9/15	0.28	0.50	-51.34	22	-55.3
NEWGYP L6 29/4/16	0.14	0.23	-51.11	14	-52.8
NEWGYP L4 4/5/16	0.30	0.52	-50.81	23	-54.5
NEWGYP L3 5/5/16	0.29	0.49	-51.27	25	-55.2
NEWGYP L4 11/5/16 (1)	0.21	0.36	-50.80	18	-53.7
NEWGYP L5 12/5/16	0.08	0.14	-51.81	10	-52.9
NEWGYP L6 13/5/16	0.17	0.30	-51.77	10	-54.2
NEWGYP L1 10/6/16 (1)	0.19	0.31	-50.78	22	-53.3
NEWGYP L2 11/6/16 (2)	0.17	0.31	-51.88	9	-54.4
NEWGYP L4 17/8/16	0.20	0.35	-50.59	16	-52.9
1σ	**0.07**	**0.12**	**0.63**	**6**	**1.0**

INTERNAL PRECISION	$\delta^{17}O$	$\delta^{18}O$	δD	^{17}O-excess	d-excess
SPIT	-0.07	-0.12	-0.66	-8	0.3
SPIT	0.03	0.06	0.44	0	0.0
SPIT	0.03	0.08	0.63	-11	0.0
SPIT	-0.02	-0.02	0.76	-11	0.9
SPIT	-0.06	-0.09	-0.75	-14	0.0
SPIT	0.03	0.06	-0.01	-3	-0.5
SPIT	0.02	0.05	-0.66	-5	-0.8
SPIT	0.05	0.12	-0.09	-9	-1.1
SPIT	0.04	0.06	-0.04	4	-0.6
SPIT	-0.08	-0.14	-0.60	-5	0.9
SPIT	0.01	-0.01	-1.65	13	-1.6
SPIT	0.02	0.04	0.32	-1	0.0
SPIT	-0.06	-0.11	-0.65	-4	0.2
SPIT	0.01	0.02	0.09	-5	-0.1
SPIT	0.06	0.11	0.26	-2	-0.6
SPIT	0.00	-0.01	-1.03	3	-1.0
SPIT	-0.08	-0.15	-0.60	1	1.1
SPIT	-0.01	0.00	0.23	-15	0.2
SPIT	0.00	0.01	0.18	-3	0.1
SPIT	0.00	0.01	0.24	-2	0.1
SPIT	-0.01	0.00	0.19	-12	0.2
SPIT	-0.07	-0.13	-0.59	-7	0.4
SPIT	0.01	0.03	0.40	-8	0.2
SPIT	-0.05	-0.08	-0.47	-11	0.2
SPIT	0.00	0.02	-0.61	-6	-1.0
SPIT	-0.06	-0.09	-0.61	-16	0.1
SPIT	-0.07	-0.08	-0.62	-25	0.1
SPIT	-0.01	-0.01	-0.45	-9	-0.3
SPIT	-0.06	-0.10	-0.66	-8	0.2
SPIT	0.08	0.15	0.45	-2	-0.8
SPIT	0.04	0.08	-1.07	3	-1.7
SPIT	-0.03	-0.05	-1.02	-5	-0.6
SPIT	-0.01	-0.01	-0.30	-4	-0.2
1σ	**0.04**	**0.08**	**0.57**	**7**	**0.7**

Table S3:

Stable isotope ratios of lake waters from the Yucatán Peninsula.

Sample	$\delta^{17}O$	(1σ)	$\delta^{18}O$	(1σ)	δD	(1σ)	d-excess	^{17}O-excess	Latitude (N)	Longitude (W)
Lake Chichancanab										
Chichancanab 09-XI-04 2 m	1.55	0.04	2.98	0.04	13.34	0.25	-10.5	-20	19° 52.771'	88° 46.026'
Chichancanab 09-XI-04 3 m	1.40	0.01	2.70	0.02	10.39	0.11	-11.2	-25	19° 52.771'	88° 46.026'
Chichancanab 09-XI-04 12 m	1.43	0.02	2.76	0.03	11.18	0.16	-10.9	-29	19° 52.771'	88° 46.026'
Chichancanab 27-II-05 A	1.76	0.03	3.41	0.04	13.08	0.32	-14.2	-41	19° 52.771'	88° 46.026'
Chichancanab 27-II-05	1.90	0.02	3.68	0.03	15.31	0.16	-14.2	-40	19° 52.771'	88° 46.026'
Chichancanab #1 B SURF	1.78	0.03	3.44	0.04	14.67	0.19	-12.8	-32	19° 52.771'	88° 46.026'
Chichancanab DEEP #2 A	1.76	0.02	3.39	0.02	14.59	0.11	-12.5	-28	19° 52.771'	88° 46.026'
Chichancanab DEEP #2B	1.76	0.01	3.40	0.04	14.47	0.14	-12.7	-31	19° 52.771'	88° 46.026'
Chichancanab DEEP #5 B	1.76	0.02	3.38	0.02	14.31	0.15	-12.8	-25	19° 52.771'	88° 46.026'
Chichancanab DEEP 13 #5	1.76	0.02	3.41	0.03	14.30	0.09	-13.0	-36	19° 52.771'	88° 46.026'
Chichancanab 22-V-00 A	1.97	0.03	3.82	0.04	17.21	0.09	-13.4	-42	19° 52.771'	88° 46.026'
Chichancanab 22-V-00 B	1.65	0.03	3.20	0.03	13.37	0.15	-12.7	-36	19° 52.771'	88° 46.026'
Chichancanab 19-VI-96	1.32	0.03	2.56	0.04	10.13	0.17	-10.5	-30	19° 52.771'	88° 46.026'
CH Lake water surface #1A	1.79	0.03	3.45	0.02	14.86	0.12	-12.7	-28	19° 52.771'	88° 46.026'
CH 8-III-04 0m	1.55	0.04	2.98	0.06	11.95	0.29	-11.6	-23	19° 52.771'	88° 46.026'
CH 8-III-04 1m	1.54	0.02	2.95	0.03	12.16	0.19	-11.1	-21	19° 52.771'	88° 46.026'
CH 8-III-04 2m	1.49	0.02	2.86	0.03	11.73	0.10	-10.8	-24	19° 52.771'	88° 46.026'
CH 8-III-04 3m	1.38	0.03	2.67	0.04	10.39	0.16	-11.0	-32	19° 52.771'	88° 46.026'
CH 8-III-04 4m	1.36	0.03	2.62	0.04	10.08	0.17	-10.9	-23	19° 52.771'	88° 46.026'
CH 8-III-04 5m	1.49	0.03	2.87	0.04	11.73	0.17	-11.2	-19	19° 52.771'	88° 46.026'
CH 8-III-04 6m	1.49	0.03	2.86	0.04	11.80	0.23	-11.1	-19	19° 52.771'	88° 46.026'
CH 8-III-04 8m	1.51	0.04	2.91	0.06	12.04	0.35	-11.2	-21	19° 52.771'	88° 46.026'
CH 8-III-04 10m	1.50	0.03	2.89	0.05	11.80	0.18	-11.3	-25	19° 52.771'	88° 46.026'
CH 8-III-04 12m	1.38	0.03	2.67	0.03	10.37	0.23	-11.0	-26	19° 52.771'	88° 46.026'
CH 8-III-04 14m	1.44	0.02	2.77	0.03	11.47	0.21	-10.7	-21	19° 52.771'	88° 46.026'
Peten Itza Lake										
PI 13-VIII-02 0 m	1.53	0.03	2.94	0.03	16.05	0.21	-7.5	-23	17° 0.170'	89° 47.956'
PI 13-VIII-02 0 m II	1.54	0.03	2.95	0.04	15.34	0.15	-8.3	-21	17° 0.170'	89° 47.956'
PI 13-VIII-02 10 m	1.54	0.03	2.95	0.03	16.31	0.16	-7.3	-16	17° 0.170'	89° 47.956'
PI 13-VIII-02 10 m II	1.56	0.03	3.00	0.05	15.56	0.10	-8.4	-25	17° 0.170'	89° 47.956'
PI 13-VIII-02 20 m	1.50	0.06	2.85	0.10	15.50	0.52	-7.3	-8	17° 0.170'	89° 47.956'
PI 13-VIII-02 20 m II	1.54	0.03	2.95	0.03	15.47	0.10	-8.2	-18	17° 0.170'	89° 47.956'
PI 13-VIII-02 30 m	1.45	0.03	2.78	0.07	15.51	0.38	-6.7	-14	17° 0.170'	89° 47.956'
PI 13-VIII-02 30 m II	1.42	0.03	2.73	0.03	14.21	0.17	-7.6	-19	17° 0.170'	89° 47.956'
PI 13-VIII-02 40 m	1.43	0.04	2.75	0.04	14.98	0.29	-7.0	-24	17° 0.170'	89° 47.956'
PI 13-VIII-02 40 m II	1.44	0.03	2.79	0.03	14.50	0.09	-7.8	-32	17° 0.170'	89° 47.956'
PI 13-VIII-02 60 m	1.42	0.04	2.74	0.05	15.19	0.27	-6.7	-24	17° 0.170'	89° 47.956'
PI 13-VIII-02 60 m II	1.43	0.02	2.75	0.04	14.45	0.11	-7.6	-19	17° 0.170'	89° 47.956'
PI 13-VIII-02 90 m	1.34	0.03	2.59	0.07	14.28	0.54	-6.4	-29	17° 0.170'	89° 47.956'
PI 13-VIII-02 90 m II	1.38	0.04	2.65	0.04	13.17	0.14	-8.1	-22	17° 0.170'	89° 47.956'
PI 13-VIII-02 120 m	1.41	0.05	2.72	0.08	15.01	0.49	-6.8	-27	17° 0.170'	89° 47.956'
PI 13-VIII-02 120 m II	1.34	0.01	2.58	0.02	12.85	0.10	-7.8	-26	17° 0.170'	89° 47.956'
PI 13-VIII-02 150 m	1.40	0.04	2.68	0.05	14.68	0.31	-6.8	-17	17° 0.170'	89° 47.956'
PI 13-VIII-02 150 m II	1.41	0.03	2.71	0.04	14.01	0.17	-7.7	-22	17° 0.170'	89° 47.956'
PI1 06-VIII-02-0m	1.58	0.03	3.01	0.04	15.74	0.14	-8.3	-10	17° 0.170'	89° 47.956'
PI1 06-VIII-02-5m	1.48	0.02	2.83	0.02	15.04	0.10	-7.6	-15	17° 0.170'	89° 47.956'
PI1 06-VIII-02-10m	1.47	0.03	2.81	0.03	14.90	0.11	-7.6	-14	17° 0.170'	89° 47.956'
PI1 06-VIII-02-15m	1.16	0.02	2.23	0.02	12.62	0.16	-5.2	-11	17° 0.170'	89° 47.956'
PI1 06-VIII-02-20m	1.10	0.02	2.10	0.02	11.79	0.11	-5.0	-14	17° 0.170'	89° 47.956'
PI5 06-VIII-02-0m	1.44	0.02	2.77	0.02	15.00	0.08	-7.2	-23	17° 0.170'	89° 47.956'
PI5 06-VIII-02-5m	1.51	0.01	2.90	0.03	15.46	0.17	-7.7	-17	17° 0.170'	89° 47.956'
PI5 06-VIII-02-10m	1.49	0.02	2.85	0.02	15.62	0.05	-7.2	-18	17° 0.170'	89° 47.956'
PI2-06-VIII-02-0m	1.45	0.02	2.79	0.03	14.95	0.12	-7.4	-20	17° 0.170'	89° 47.956'
PI17-06-VIII-02-0m	1.50	0.03	2.85	0.03	15.22	0.10	-7.6	0	17° 0.170'	89° 47.956'
PI17-06-VIII-02-7m	1.47	0.03	2.81	0.03	14.97	0.08	-7.5	-13	17° 0.170'	89° 47.956'
PI13-06-VIII-02-150m	1.45	0.01	2.74	0.03	15.01	0.14	-6.9	-1	17° 0.170'	89° 47.956'
PI07-06-VIII-02-0m	1.24	0.02	2.39	0.02	11.91	0.08	-7.2	-22	17° 0.170'	89° 47.956'
PI07-06-VIII-02-7m	1.39	0.03	2.66	0.02	14.00	0.18	-7.3	-18	17° 0.170'	89° 47.956'
Lake Peten #193 B 12-VIII-2005	1.53	0.02	2.94	0.04	15.56	0.14	-7.9	-19	17° 0.170'	89° 47.956'
Peten Itza Lake 6-VII-1995 core site surface	1.39	0.03	2.69	0.07	13.86	0.38	-8.1	-31	17° 0.170'	89° 47.956'
Peten Itza Remate PI-22-VIII-99 core site	1.51	0.04	2.95	0.04	14.89	0.24	-8.7	-41	17° 0.170'	89° 47.956'
Peten Itza Central 29-VIII-99 surf	1.57	0.03	3.02	0.02	15.86	0.42	-8.9	-25	17° 0.170'	89° 47.956'
Salpeten Lake										
SP-13-VI-02 0m ST1 A A	2.22	0.03	4.23	0.04	20.13	0.32	-13.7	-13	16°58.8'	89°40.0'
SP-13-VI-02 2m ST1 A B	2.23	0.02	4.26	0.02	20.62	0.14	-13.5	-22	16°58.8'	89°40.0'
SP 13-07-02 5 m STIA	2.24	0.05	4.31	0.10	20.23	0.41	-14.3	-36	16°58.8'	89°40.0'
SP-13-VI-02 10m ST1 A A	2.23	0.04	4.27	0.08	21.28	0.45	-12.9	-19	16°58.8'	89°40.0'
SP-13-VI-02 15m ST1 A B	2.09	0.04	4.01	0.06	19.99	0.44	-12.1	-19	16°58.8'	89°40.0'
SP-13-VI-02 20m ST1 A B	2.07	0.02	3.97	0.03	19.95	0.15	-11.8	-27	16°58.8'	89°40.0'
SP-13-VI-02 30m ST1 A A	1.87	0.03	3.59	0.04	16.67	0.21	-12.1	-25	16°58.8'	89°40.0'
SP shore 10-VIII- 2005	2.16	0.02	4.18	0.02	18.32	0.40	-14.9	-44	16°58.8'	89°40.0'
Salpeten 20-I-2006 #210	2.45	0.02	4.70	0.03	23.06	0.37	-14.5	-31	16°58.8'	89°40.0'
SP2 19-VIII-99 bottom 16 m	1.93	0.03	3.70	0.03	16.23	0.11	-13.3	-27	16°58.8'	89°40.0'
Xcaamal Lake										
XCA 30-VIII-2 0m	1.08	0.03	2.06	0.05	3.36	0.30	-13.1	-8	20° 36.599'	89° 42.907'
XCA 30-VIII-2 2m	0.89	0.04	1.68	0.04	1.87	0.33	-11.6	-3	20° 36.599'	89° 42.907'
XCA 30-VIII-2 4m	0.93	0.02	1.80	0.03	3.20	0.19	-11.2	-17	20° 36.599'	89° 42.907'
XCA 30-VIII-2 6m	0.90	0.04	1.73	0.07	3.19	0.32	-10.7	-13	20° 36.599'	89° 42.907'
XCA 30-VIII-2 8m	0.91	0.02	1.74	0.04	3.52	0.13	-10.4	-8	20° 36.599'	89° 42.907'
XCA 30-VIII-02 10 m	1.01	0.03	1.90	0.02	4.59	0.13	-10.6	7	20° 36.599'	89° 42.907'
XCA 30-VIII-02	1.02	0.02	1.95	0.02	5.08	0.07	-10.5	-9	20° 36.599'	89° 42.907'
XCA 5-III-04 0m	0.87	0.03	1.67	0.05	3.14	0.29	-10.2	-11	20° 36.599'	89° 42.907'
XCA 5-III-04 1m	0.52	0.02	1.03	0.04	-2.53	0.15	-10.8	-19	20° 36.599'	89° 42.907'
XCA 5-III-04 2m	0.38	0.03	0.74	0.04	-5.56	0.25	-11.5	-16	20° 36.599'	89° 42.907'
XCA 5-III-04 3m	0.46	0.04	0.88	0.07	-1.78	0.36	-8.8	-4	20° 36.599'	89° 42.907'
XCA 5-III-04 4m	0.41	0.04	0.78	0.07	-1.81	0.18	-8.0	0	20° 36.599'	89° 42.907'
XCA 5-III-04 5m	0.78	0.03	1.48	0.06	2.20	0.32	-9.6	-3	20° 36.599'	89° 42.907'
XCA 5-III-04 6m	0.19	0.02	0.38	0.01	-5.13	0.07	-8.2	-15	20° 36.599'	89° 42.907'
XCA 5-III-04 7m	0.43	0.01	0.86	0.01	-4.36	0.14	-11.2	-26	20° 36.599'	89° 42.907'
XCA 5-III-04 8m	0.36	0.02	0.70	0.04	-2.47	0.24	-8.0	-7	20° 36.599'	89° 42.907'
XCA 5-III-04 9m	0.21	0.05	0.43	0.06	-5.53	0.30	-9.0	-15	20° 36.599'	89° 42.907'
XCA 5-III-04 10m	0.46	0.03	0.87	0.04	-0.99	0.27	-8.0	-6	20° 36.599'	89° 42.907'
XCA 5-III-04 11m	0.46	0.03	0.88	0.06	-1.25	0.27	-8.3	-9	20° 36.599'	89° 42.907'
CXCA 5III 04 Cladium H2O	0.64	0.03	1.27	0.04	1.11	0.34	-9.1	-29	20° 36.599'	89° 42.907'
Xcaamal A 26-II-05	1.03	0.03	1.99	0.06	4.58	0.51	-11.3	-15	20° 36.599'	89° 42.907'
Xcaamal 08-VIII-01 used to cond	1.28	0.03	2.51	0.06	7.39	0.27	-12.6	-39	20° 36.599'	89° 42.907'

Table S3 Continued:

Sample	$\delta^{17}O$	(1σ)	$\delta^{18}O$	(1σ)	δD	(1σ)	d-excess	^{17}O-excess	Latitude (N)	Longitude (W)
San Jose Lake										
SJ 4-III-04 0m	-0.41	0.02	-0.75	0.02	-8.06	0.18	-2.1	-10	20° 52.316'	90° 8.252'
SJ 4-III-04 1m	-0.45	0.02	-0.86	0.03	-8.94	0.07	-2.0	4	20° 52.316'	90° 8.252'
SJ 4-III-04 2m	-0.16	0.02	-0.33	0.03	-4.60	0.13	-1.9	17	20° 52.316'	90° 8.252'
SJ 4-III-04 3m	-0.31	0.03	-0.63	0.03	-6.91	0.16	-1.9	19	20° 52.316'	90° 8.252'
SJ 4-III-04 4m	-0.37	0.03	-0.72	0.04	-7.08	0.14	-1.3	15	20° 52.316'	90° 8.252'
SJ 4-III-04 5m	-0.28	0.02	-0.55	0.02	-5.71	0.22	-1.3	10	20° 52.316'	90° 8.252'
SJ 4-III-04 6m	-0.25	0.02	-0.50	0.03	-5.41	0.08	-1.4	10	20° 52.316'	90° 8.252'
SJ 04-II-04 7 m	-0.35	0.01	-0.65	0.03	-6.31	0.17	-1.1	-5	20° 52.316'	90° 8.252'
SJ 4-III-04 8m	-0.23	0.02	-0.46	0.02	-5.07	0.07	-1.4	8	20° 52.316'	90° 8.252'
SJ 4-III-04 9m	-0.18	0.02	-0.37	0.02	-4.73	0.08	-1.8	11	20° 52.316'	90° 8.252'
SJ 4-III-04 10m	-0.29	0.03	-0.58	0.03	-6.57	0.14	-2.0	15	20° 52.316'	90° 8.252'
San Jose B surface #5	0.09	0.03	0.17	0.03	-3.87	0.09	-5.3	1	20° 52.316'	90° 8.252'
Punta Laguna										
Punta Laguna 3-IV-05	1.32	0.03	2.58	0.04	11.42	0.09	-9.4	-41	20° 38.888'	87° 38.128'
Punta Laguna 26-V-00 mid basin	0.76	0.02	1.45	0.03	5.83	0.17	-5.8	-6	20° 38.888'	87° 38.128'
Punta Laguna 26-V-00 east basin	1.05	0.03	2.00	0.05	8.40	0.17	-7.6	-8	20° 38.888'	87° 38.128'
Punta Laguna 3-VI-95	0.88	0.03	1.69	0.03	5.64	0.28	-8.9	-12	20° 38.888'	87° 38.128'
Punta Laguna 20-I-96 end of the dock	0.20	0.03	0.41	0.04	0.40	0.16	-3.9	-16	20° 38.888'	87° 38.128'
Punta Laguna 2-5-96	0.22	0.02	0.45	0.05	0.05	0.33	-4.5	-18	20° 38.888'	87° 38.128'
Other lakes										
Sacnab surf water 13-VIII-03	2.16	0.05	4.11	0.06	22.07	0.12	-10.8	-8	17° 03.0'	89° 22.0'
Sacnab west end 31-VIII-99	1.39	0.03	2.68	0.03	12.04	0.13	-9.3	-22	17° 03.0'	89° 22.0'
Lake Petenxil surface 16-VIII-03	2.12	0.02	4.05	0.02	15.03	0.17	-17.4	-16	17° 0.170'	89° 47.956'
Sayacil # 2 deep	2.28	0.02	4.38	0.03	16.29	0.17	-18.8	-26	20° 41.037'	88° 48.73'
Sayaucil surface A #6	2.70	0.02	5.18	0.04	19.79	0.19	-21.6	-28	20° 41.037'	88° 48.73'
Sayaucil #2 deep	2.35	0.03	4.54	0.04	17.14	0.31	-19.2	-47	20° 41.037'	88° 48.73'
Sayaucil #6 surface	2.65	0.02	5.11	0.05	19.73	0.15	-21.1	-41	20° 41.037'	88° 48.73'
Yalahau #5	1.66	0.03	3.21	0.03	14.30	0.16	-11.3	-29	20° 39.4'	89° 13.1'
Lake Sacpuy Surface	1.46	0.02	2.84	0.03	9.68	0.28	-13.0	-39	16° 59.4'	90° 3.1'
Lake Sacpuy Surface 16-VIII-03	2.43	0.02	4.69	0.02	22.07	0.38	-15.5	-39	16° 59.4'	90° 3.1'
Lake Yaxha 13-8-03 4.2 m	1.72	0.04	3.29	0.04	16.31	0.21	-10.0	-12	17° 3.5'	89°24.5'
Tikal Aguada 13-VIII-01	2.68	0.02	5.14	0.03	19.46	0.15	-21.6	-30	17° 13.741'	89° 36.131'
Lake Quexil 16-VIII-03 surface	2.16	0.02	4.16	0.03	17.95	0.14	-15.3	-32	16° 55.5'	89° 48.1'
Uaxactun Aguada 13-VIII-01	0.57	0.03	1.10	0.04	-1.43	0.13	-10.2	-12	17° 23.643'	89° 38.077'
Santa Ana Vieja Aguada 14-VIII-01	-0.36	0.02	-0.66	0.04	-4.87	0.21	0.4	-8	16° 38.6'	89° 45.0'
Aguada Zacpeten 30-I-2006	2.64	0.03	5.08	0.03	21.87	0.40	-18.8	-36	16° 59.255'	89° 39.602'
Laguna Milagros 15-V-02	1.23	0.03	2.34	0.04	11.42	0.34	-7.3	-6	18° 30.2'	88° 25.5'
Sayil little basin 4-III-05	1.92	0.02	3.69	0.04	14.29	0.21	-15.2	-21	20° 10.684'	89° 39.128'
Laguna near Xcaamal A 31-III-05	1.39	0.03	2.67	0.04	15.17	0.34	-6.5	-20	20° 36.599'	89° 42.907'
Laguna near Xcaamal B 31-III-05	1.40	0.03	2.71	0.04	15.66	0.16	-13.8	-35	20° 36.599'	89° 42.907'
Cenote 05-III-04 261B 0m	2.42	0.01	4.65	0.02	18.69	0.16	-18.5	-29	20° 35.707'	89° 42.70'
Cenote 261 A Surf	3.01	0.02	5.82	0.05	23.21	0.32	-23.3	-57	20° 35.707'	89° 42.70'
Cenote 261 95B 2-VIII-2005	1.69	0.02	3.26	0.02	9.98	0.17	-16.1	-27	20° 35.707'	89° 42.70'
Cenote 261 B 26-II-05	2.59	0.01	4.98	0.03	20.23	0.23	-19.6	-37	20° 35.707'	89° 42.70'
Cenote 261 26-II-05	2.35	0.04	4.55	0.05	18.19	0.11	-18.3	-48	20° 35.707'	89° 42.70'
Cenote 261 21-VIII-05	1.23	0.02	2.43	0.03	4.78	0.06	-14.6	-47	20° 35.707'	89° 42.70'
Quexil shore 7-III-2005	2.03	0.05	3.93	0.07	17.57	0.49	-13.8	-36	20° 35.707'	89° 42.70'
Cenote X'caamal #96B 2-VIII-2005	0.63	0.02	1.22	0.03	-0.55	0.09	-10.3	-13	20° 35.707'	89° 42.70'
Monifata 7-VIII-97	0.79	0.02	1.52	0.05	2.66	0.25	-9.5	-10	16° 55.343'	89° 50.247'
La Gloria 21-VIII-09	0.87	0.02	1.72	0.05	3.80	0.33	-10.0	-36	16° 56.745'	90° 22.495'
Uxmal Fountain	0.10	0.03	0.20	0.03	-1.45	0.18	-3.0	-3	20° 21.672'	89° 46.091'
Yalahau surface #3 B	1.62	0.05	3.10	0.06	12.74	0.52	-12.1	-20	20° 39.447'	89° 12.979'
Yalahau deep #1 A	1.62	0.04	3.13	0.04	13.22	0.28	-11.8	-37	20° 39.447'	89° 12.979'
Well Macanche 28-VIII-99	1.46	0.02	2.80	0.03	13.31	0.25	-9.1	-23	16° 58.0'	89° 38.5'
Macanche surface 28-VIII-99	1.62	0.04	3.12	0.06	14.28	0.45	-10.7	-30	16° 58.0'	89° 38.5'
Amatitlan 13-III-2000 1m	-2.57	0.03	-4.91	0.03	-39.95	0.12	-0.7	28	14° 28.908'	90° 36.103'
Amatitlan 14-III-2000 core site	-1.63	0.03	-3.09	0.05	-29.25	0.26	-4.5	4	14° 28.908'	90° 36.103'
Amatitlan 15-III-2000 core site	-2.77	0.04	-5.28	0.09	-42.11	0.51	0.1	23	14° 28.908'	90° 36.103'
Amatitlan 14-III-2000 hot spring	-2.98	0.05	-5.66	0.08	-48.06	0.65	-3.1	14	14° 28.908'	90° 36.103'
Coba deep #5	1.31	0.03	2.51	0.04	11.41	0.23	-8.6	-14	20° 29.652'	87° 44.308'
Coba deep #2	1.27	0.01	2.43	0.02	11.22	0.17	-8.3	-11	20° 29.652'	87° 44.308'
Coba surface #1A	1.30	0.03	2.47	0.04	10.86	0.16	-8.9	-8	20° 29.652'	87° 44.308'
Coba surface #1	1.26	0.01	2.41	0.02	10.81	0.15	-8.5	-9	20° 29.652'	87° 44.308'
Lake Coba 2-V-96	-0.15	0.02	-0.25	0.04	-3.69	0.17	-2.6	-16	20° 29.652'	87° 44.308'
L. Coba 2-VI-96	0.54	0.02	1.03	0.02	2.75	0.14	-5.5	0	20° 29.652'	87° 44.308'

Table S4: Stable isotope ratios of river and freshwaters from the Yucatán Peninsula.

Sample	$\delta^{17}O$	(1σ)	$\delta^{18}O$	(1σ)	δD	(1σ)	d-excess	^{17}O-excess	Latitude (N)	Longitude (W)
Bladen River, Toledo, 13-I-02	-2.18	0.03	-4.14	0.02	-21.31	0.08	11.8	7	16° 28.290'	88° 38.766'
Rio Blanco, Toledo, BZ, 11-I-02	-2.09	0.03	-3.96	0.05	-21.07	0.15	10.6	5	15° 19.941'	91° 0.104'
Sibun River, Cayo, BZ 14-I-02	-2.19	0.04	-4.15	0.06	-19.47	0.27	13.7	2	17° 6.566'	88° 39.601'
South Stann Creek, BZ, 13-1I-02	-2.07	0.03	-3.93	0.02	-19.20	0.12	12.3	5	16° 43.449'	88° 25.820'
Rio Sibun 21-VIII-01	-1.64	0.02	-3.10	0.03	-16.67	0.12	8.2	-1	17° 6.566'	88° 39.601'
Rio Dolores 21-VIII-01	-2.35	0.02	-4.47	0.04	-21.20	0.34	14.6	11	15° 41.012'	90° 24.513'
San Simon V 21-VIII-01	-2.59	0.03	-4.93	0.05	-26.00	0.39	13.4	14	15° 50.078'	90° 17.245'
Uspantan 20-VIII-01	-4.68	0.03	-8.90	0.03	-58.81	0.25	12.4	32	15° 19.684'	90° 57.355'
Arroyo 21-VIII-01	-1.80	0.03	-3.45	0.04	-18.74	0.31	8.9	20	16° 24.445'	90° 6.651'
Rio Candelaria 21-VIII-01	-2.10	0.04	-4.00	0.05	-20.30	0.23	11.7	16	15° 53.068'	90° 11.245'
Seasonal wetland Peten 21-VIII-01	-1.23	0.02	-2.36	0.02	-9.20	0.13	9.7	20	16° 8.675'	90° 10.833'
Rio Passion 21-VIII-01	-1.83	0.04	-3.50	0.04	-16.41	0.22	11.6	19	16° 31.868'	90° 11.313'
Coban Rio Cahabon 21-VIII-01	-3.56	0.04	-6.76	0.07	-41.11	0.18	13.0	19	15° 27.926'	90° 22.339'
Rio Ixlu 13-VIII-01	-2.00	0.04	-3.81	0.05	-24.09	0.24	6.4	11	16° 58.460'	89° 41.199'
Rio Dulce 14-VIII-01	-1.70	0.04	-3.26	0.07	-17.37	0.21	8.7	25	15° 39.438'	89° 0.014'
Rio Ixbobo 14-VIII-01	-1.83	0.04	-3.48	0.04	-16.94	0.20	10.9	6	16° 8.866'	89° 24.167'
Town of Copan Rio Aguas Calientes 15-VIII-01	-2.92	0.03	-5.50	0.04	-31.20	0.23	12.8	-9	14° 50.434'	89° 9.212'
Rio Copan at site 15-VIII-01	-3.09	0.02	-5.87	0.04	-33.42	0.30	13.6	12	14° 50.011'	89° 8.487'
Rio Machaquila 14-VIII-01	-1.78	0.03	-3.34	0.04	-18.66	0.18	8.1	-8	16° 23.612'	89° 26.615'
Rio Cienega 15-VIII-01	-1.49	0.02	-2.81	0.02	-11.84	0.06	10.6	-1	15° 44.074'	89° 4.626'
Rio San Pedro 14-VIII-01	-1.68	0.02	-3.18	0.02	-13.79	0.26	11.7	-4	15° 56.833'	89° 14.697'
Rio San Juan 14-VIII-01	-2.06	0.01	-3.90	0.03	-19.93	0.34	11.3	7	16° 37.871'	89° 36.251'
Rio Camotan 15-VIII-01	-3.14	0.03	-5.95	0.03	-36.06	0.25	11.6	13	14° 51.300'	89° 19.424'
Rio Matagun 15-VIII-01	-3.90	0.04	-7.38	0.05	-48.48	0.26	10.6	1	14° 58.6'	89° 31.45'
Cenote Cristal 11-VIII-01	-2.23	0.02	-4.27	0.03	-25.04	0.30	9.1	25	20° 35.707'	89° 42.70'
Cenote Aktun Ha	-2.14	0.02	-4.08	0.05	-23.60	0.25	9.0	19	20° 35.707'	89° 42.70'
Cenote Ik Kil near Chichen 12-VIII-01	-2.06	0.03	-3.90	0.04	-21.87	0.19	9.4	0	20° 35.707'	89° 42.70'
Celestun Cenote 18-VIII-94	-0.59	0.02	-1.13	0.02	-6.01	0.22	3.0	7	20° 35.707'	89° 42.70'
Rio Grande 15-VIII-01	-3.01	0.02	-5.73	0.03	-36.49	0.39	9.4	18	14° 57.278'	89° 32.231'
Kikil 21-VI-94	-1.30	0.03	-2.49	0.06	-13.56	0.22	6.4	14	21° 11.511'	88° 10.117'
Bacalar surface 12-VI-02	-1.27	0.04	-2.46	0.06	-15.16	0.15	4.5	35	18° 39.100'	88° 24.522'
Cenote Azul Bacalar 12-VI-02	-2.04	0.03	-3.89	0.05	-24.26	0.15	6.9	16	18° 39.100'	88° 24.522'
E of Paxcaman #142 Source 1-XIII-2005	-1.55	0.05	-2.97	0.07	-15.91	0.40	8.0	12	16° 56.7'	89° 46.3'
Xcambo water sample paso B 3-III-05	-2.05	0.04	-3.90	0.07	-22.71	0.46	8.5	6	21° 18.54'	89° 21.11'
Xcambo 2nd pool A 3-III-05	-1.11	0.02	-2.16	0.03	-14.69	0.25	2.6	28	21° 18.54'	89° 21.11'
Xcambo, paso 3-III-05	-2.09	0.02	-3.98	0.04	-23.85	0.36	8.0	7	21° 18.54'	89° 21.11'
Rio Lagartos Cenote	-1.49	0.03	-2.83	0.05	-15.21	0.18	7.4	6	21° 35.759'	88° 8.745'
Telchaquillo Cenote 29-III-05	-2.18	0.04	-4.18	0.04	-24.54	0.15	8.9	26	20° 38.58'	89° 27.29'
Mayapan drip 3-4-5 29-III-05	-2.15	0.02	-4.11	0.03	-25.06	0.26	7.8	18	20° 37.751'	89° 27.631'
Cenote Chi-Huan Holca 30-III-05	-2.25	0.02	-4.27	0.05	-26.76	0.07	7.4	8	20° 45'46	88° 55.52
Mayapan pool watertable A 2-III-05	-2.32	0.02	-4.42	0.04	-25.88	0.15	9.5	19	20° 28.564'	89° 11.864'
Mayapan dripwater2 29-II-05	-1.81	0.02	-3.47	0.02	-22.35	0.31	5.4	23	20° 37.751'	89° 27.631'
Mayapan dripwater2 29-II-05	-1.81	0.02	-3.47	0.02	-22.35	0.31	5.4	23	20° 37.751'	89° 27.631'
Calcehtok 2 25-II-05	-1.32	0.03	-2.49	0.02	-9.86	0.26	9.9	-1	20° 33.052'	89° 54.733'
Calcehtok 3 pool	-1.42	0.02	-2.70	0.02	-14.36	0.12	6.9	10	20° 33.052'	89° 54.733'
Rio Ixtul 7-VIII-2005 #146	-1.94	0.03	-3.69	0.05	-20.74	0.19	8.5	13	20° 55.37	87° 7.39
Rio Ixtul 7-VIII-2005 #146	-1.95	0.03	-3.68	0.05	-20.60	0.12	9.0	-5	20° 55.38	87° 7.40
Calcehtok 4 cascada	-1.58	0.02	-3.00	0.03	-14.40	0.11	9.8	9	20° 33.041'	89° 54.740'
Calcehtok 3 pool	-1.43	0.02	-2.69	0.02	-14.02	0.13	7.4	-7	20° 33.041'	89° 54.740'
Calcehtok drip 3	-1.87	0.03	-3.54	0.04	-19.64	0.26	8.7	-3	20° 33.041'	89° 54.740'
Rio Madre Vieja 18-VIII-01	-3.21	0.03	-6.08	0.04	-43.25	0.37	5.5	6	16° 41.818'	89° 44.859'
Rio Benque Viejo 16-VIII-01	-3.67	0.04	-6.96	0.05	-51.06	0.18	4.6	7	17° 4.264'	89° 8.374'
Rio Asuchillo 17-VIII-01	-3.06	0.02	-5.82	0.02	-36.58	0.12	10.1	15	15° 19.941'	91° 0.104'
Rio Blanco 20-VIII-01	-4.77	0.02	-9.05	0.03	-62.84	0.07	9.7	10	15° 19.941'	91° 0.104'
Rio Hato 16-VIII-01	-4.10	0.02	-7.79	0.03	-52.61	0.08	9.9	12	15° 19.941'	91° 0.104'
L Catemaco, MX 21-V-03 01F2	-1.06	0.01	-2.03	0.03	-7.50	0.17	8.77	13	18° 25.44'	95° 7.54'
L. Izabal 3-VI-02	-1.51	0.04	-2.90	0.02	-14.98	0.40	8.0	8	15° 38.052'	88° 59.491'
Edzna water bath #105 2-VIII-05	-2.04	0.02	-3.90	0.03	-24.26	0.28	6.9	17	19° 35.51'	90° 13.42'
Uxmal Fountain	0.12	0.04	0.20	0.08	-1.57	0.19	-3.2	15	20° 21.39'	89° 45.58'
Jalacte Creek 08-I-02 Toledo District	-1.78	0.03	-3.40	0.06	-17.44	0.38	9.8	18	16° 10.1'	89° 4.5'
Rio Cunen El Molino 20-VIII-01	-4.70	0.03	-8.94	0.05	-61.18	0.37	10.3	24	15°17.48	91° 4.14'
Madre Vieja Trib 18-VIII-01	-2.98	0.02	-5.67	0.03	-42.81	0.36	2.5	15	16° 41.818'	89° 44.859'
CA-2 Km 90 Rio 18-VIII-01	-3.17	0.02	-6.05	0.02	-37.94	0.11	10.5	32	16° 41.818'	89° 44.859'
Rio Chixoy 20-VIII-01	-4.73	0.02	-9.00	0.02	-64.21	0.35	7.8	30	15° 21.283'	90° 39.361'
Xbuya Ha 10-VI-94 13:53	-1.34	0.03	-2.53	0.03	-14.15	0.19	6.0	-4	21° 23.41'	88° 53.42
Xbuya Ha 940614 10:30 3m VOCAL	-2.04	0.05	-3.86	0.08	-22.39	0.33	8.4	-4	21° 23.41'	88° 53.43
Noc Ac 10:30 sup 940614	-2.05	0.03	-3.87	0.07	-22.18	0.21	8.7	-6	21° 23.41'	88° 53.44
Dzibilchaltun 28-5-94 sample 1	-2.10	0.05	-3.97	0.06	-22.98	0.21	8.7	2	21° 5.30'	89° 35.48'
Dzitya cenote 18-5-96	-2.08	0.02	-3.90	0.05	-22.97	0.25	8.2	-13	21° 3.09	89° 40.53'53
Rio Lagartos Chiquila cenote 11-VI-1994	-1.49	0.04	-2.87	0.04	-17.19	0.53	5.7	24	21° 35.759'	88° 8.745'
Rio Lagartos Chiquila cenote 30-VI-1994	-1.47	0.02	-2.83	0.02	-16.56	0.23	6.1	24	21° 35.759'	88° 8.745'
Celestun Cenote 18-6-94	-0.46	0.03	-0.90	0.03	-6.08	0.06	1.1	14	20° 51.37'	90° 23.43'
Dzitnup (Xkeken) 14-VI-96	-1.94	0.05	-3.69	0.09	-21.38	0.41	8.2	16	20° 39.4'	88° 14.34'
Cenote Dziuche 25-V-96	-2.00	0.03	-3.83	0.03	-22.21	0.23	8.4	19	19° 53.57	88° 48.28
Peten Itza 31-X-99	-2.26	0.03	-4.30	0.04	-24.76	0.47	9.6	14	17° 0.170'	89° 47.956'
Cave Actuum Caan 1 #194 15-Aug-2005	-1.33	0.04	-2.51	0.04	-17.21	0.24	2.9	-5	17° 7.47'	88° 51.00'
Cave Actuum Caan 1B #194 15-Aug-2005	-1.37	0.02	-2.58	0.02	-18.30	0.16	2.3	-10	17° 7.47'	88° 51.00'
Cave Actuum Caan 2 #195 15-Aug-2005	-1.83	0.02	-3.47	0.02	-19.47	0.05	8.3	4	17° 7.47'	88° 51.00'
Cave Actuum Caan 3 B 15-Aug-05	-1.90	0.02	-3.58	0.03	-18.57	0.15	10.1	-6	17° 7.47'	88° 51.00'
Cave Tiki Tiki drip (1-2-3) 28-02-05	-0.38	0.03	-0.73	0.04	-2.65	0.16	3.2	0	19° 58.04'	88° 59.642'
Cave Tikitiki pool 28-III-14	-2.64	0.04	-5.00	0.06	-32.48	0.21	7.8	-4	19° 58.04'	88° 59.642'
Cave Tikitiki pool B 28-III-14	-2.65	0.04	-5.05	0.05	-32.73	0.51	7.6	19	19° 58.04'	88° 59.642'
Cave Ixinche water pool 1-III-05	-2.07	0.04	-3.95	0.05	-25.41	0.27	6.2	21	20° 9.608'	88° 47.624'
Cave Ixinche 2nd water sample 1-II-05	-2.40	0.02	-4.54	0.03	-26.61	0.09	9.8	0	20° 9.608'	88° 47.624'
Cave Ixinche water pool B 1-III-05	-2.05	0.02	-3.86	0.03	-26.35	0.15	4.6	-7	20° 9.608'	88° 47.624'
Cave Ixinche 2nd water sample B 1-II-05	-2.36	0.05	-4.46	0.09	-26.94	0.31	8.8	3	20° 9.608'	88° 47.624'
Loltun Cave 21-V-94 Site 1	-1.72	0.04	-3.26	0.06	-16.68	0.25	9.3	-3	20° 15.183'	89° 27.397'
Loltun Cave 21-V-94 Site 2	-2.17	0.03	-4.11	0.04	-22.68	0.31	10.2	0	20° 15.183'	89° 27.397'
Loltun Cave 21-V-94 Site 2 B	-2.14	0.02	-4.06	0.03	-23.25	0.32	9.1	9	20° 15.183'	89° 27.397'
Loltun Cave 26-V-96	-1.94	0.02	-3.67	0.04	-19.85	0.16	9.4	-1	20° 15.183'	89° 27.397'
Loltun Cave 26-II-05	-0.60	0.03	-1.13	0.03	-1.86	0.12	7.2	2	20° 15.183'	89° 27.397'
Loltun Cave B 26-II-05	-0.63	0.03	-1.20	0.02	-3.29	0.25	6.3	-2	20° 15.183'	89° 27.397'

Table S5:

Stable isotope ratios of rainwater from the Yucatán Peninsula.

Sample	$\delta^{17}O$	(1σ)	$\delta^{18}O$	(1σ)	δD	(1σ)	d-excess	^{17}O-excess	Latitude (N)	Longitude (W)
RAIN Chichancanab 7-3-94	-1.44	0.04	-2.74	0.04	-14.22	0.54	7.7	14	19° 52.771'	88° 46.026'
RAIN Chichancanab 7-3-94 B	-1.20	0.25	-2.29	0.47	-13.38	1.52	7.3	11	19° 52.771'	88° 46.026'
RAIN-9-I-2007 3:30 PM	-0.09	0.02	-0.18	0.05	13.73	0.17	15.2	6	20° 0.993'	89° 1.218'
RAIN-30-III 3:00 PM	-1.50	0.03	-2.84	0.04	-18.16	0.36	4.6	-1	20° 0.993'	89° 1.218'
RAIN-25-I-2007 7:00 PM	0.26	0.05	0.47	0.07	15.40	0.41	11.6	6	20° 0.993'	89° 1.218'
RAIN 23-II-2007 8:00 PM	-0.08	0.04	-0.15	0.06	8.66	0.26	9.9	3	20° 0.993'	89° 1.218'
RAIN 8-III-2007 8:00	-0.96	0.02	-1.84	0.01	6.51	0.10	21.2	14	20° 0.993'	89° 1.218'
RAIN 15-I-2007 9:00	0.11	0.02	0.20	0.02	13.77	0.21	12.1	2	20° 0.993'	89° 1.218'
RAIN 5-VIII-2007 8:00	-2.80	0.02	-5.33	0.04	-30.52	0.29	12.2	16	20° 0.993'	89° 1.218'
RAIN 23-VI-2007 2:40PM	-1.29	0.03	-2.45	0.02	-14.16	0.25	5.5	1	20° 0.993'	89° 1.218'
RAIN 11-V-2007 9:30 PM	0.23	0.03	0.45	0.02	12.61	0.26	9.0	-4	20° 0.993'	89° 1.218'
RAIN 08-II-2017 1:00PM	-0.02	0.02	-0.05	0.04	11.26	0.37	11.7	3	20° 0.993'	89° 1.218'
RAIN 13-I-2007 2:15AM	0.43	0.02	0.80	0.03	16.43	0.32	10.0	5	20° 0.993'	89° 1.218'
RAIN 11-V-2007 9:30 PM	0.22	0.02	0.36	0.03	11.02	0.78	8.1	8	20° 0.993'	89° 1.218'
RAIN 08-II-2017 1:00PM	-0.03	0.02	-0.11	0.04	10.50	0.28	11.4	11	20° 0.993'	89° 1.218'
RAIN 13-I-2007 2:15AM	0.46	0.03	0.83	0.06	16.37	0.28	9.7	10	20° 0.993'	89° 1.218'
RAIN 06-II-2007 6:00PM	-0.42	0.05	-0.84	0.08	9.55	0.45	16.3	16	20° 0.993'	89° 1.218'
RAIN 12-I-2007 2:30PM	0.10	0.05	0.13	0.07	14.37	0.36	13.4	13	20° 0.993'	89° 1.218'
RAIN 6-II-2007 6.00 pm	-0.38	0.02	-0.78	0.03	10.11	0.12	16.3	29	20° 0.993'	89° 1.218'
RAIN 11-II-2007 5:00 PM	-1.09	0.02	-2.10	0.02	0.79	0.09	17.6	22	20° 0.993'	89° 1.218'
RAIN 12-I-2017 2:30PM	0.08	0.02	0.12	0.04	14.23	0.12	13.26	18	20° 0.993'	89° 1.218'
RAIN 29-IV-2007	0.10	0.02	0.18	0.02	15.12	0.29	13.70	4	20° 0.993'	89° 1.218'
RAIN 31-V-2017 6:00	-3.90	0.05	-7.37	0.07	-46.60	0.61	12.38	-2	20° 0.993'	89° 1.218'
RAIN 31-VII-2005	-0.60	0.03	-1.13	0.03	4.94	0.18	13.8	-1	20° 0.993'	89° 1.218'
RAIN Roof drain 31-VII- 2005	-0.60	0.03	-1.16	0.03	4.33	0.31	13.3	16	20° 0.993'	89° 1.218'
RAIN Punta Laguna 2-VI-96	0.23	0.05	0.42	0.06	11.63	0.16	8.2	7	20° 38.888'	87° 38.128'
RAIN Calcehtok 25-II-05	-0.48	0.03	-0.92	0.03	3.04	0.05	9.9	5	20° 33.041'	89° 54.740'
RAIN Peten Itza 21-I-96	-0.74	0.03	-1.41	0.03	1.50	0.16	12.8	4	17° 0.170'	89° 47.956'
RAIN Merida 16-VI-94	-0.63	0.03	-1.16	0.05	-3.03	0.08	6.2	-17	20° 58.654'	89° 37.407'
RAIN X'Caamal 8-VIII-01	0.20	0.02	0.39	0.03	4.97	0.20	1.8	-4	20° 36.599'	89° 42.907'
RAIN Piste 9-VI-96	-3.24	0.02	-6.15	0.03	-39.02	0.50	10.2	10	20° 41.53	88° 35.22

Table S6:

Transient model parameters. See text for details of parameters.

Category	Parameter	Units	Value
Lake Evaporation	Lake Temperature	°C	25
	w	-	0.5
	V_{eq}	-	0.6
	Vapor Temperature	°C	25
	θ_{eq}	-	0.529
	θ_{kin}	-	0.518
Precipitation	$\delta^{18}O$	(per mil, VSMOW)	-4.5
	d-excess		10
	^{17}O-excess		2.5
Groundwater	$\delta^{18}O$	(per mil, VSMOW)	-4.5
	d-excess		10
	^{17}O-excess		2.5
	Ca	g/kg	0.607
	SO_4		2.455
	Na		0.2
	Mg		0.2
	K		0.011
	Cl		0.234
Fluxes	F_p	m water equivalent/m^2/a	Reanalysis data = ~1
	F_e		1.07
	F_{gb}	kg (~m water equivalent/m^2/a)	1.02e9 (~0.1)
	F_{bg}		1.02e9 (~0.1)
	F_{b1b2}		1.02e10 (~1.0)
	F_{b2b1}		1.02e10 (~1.0)

Table S7:

Paleo-lake temperature calculations. The equation of Grossman and Ku (*45*) was used to calculate the temperature at which the aragonitic shells of *Pyrgophorus coronatus* formed.

Sample	$\delta^{18}O$ (Carbonate)	$\delta^{18}O$ (GHW)	Temperature (°C)
CHI 07-III-04 139.5-140.0 cm	3.40	4.07	24.9
CHI 07-III-04 133.0-133.5 cm	2.96	3.65	25.0
CHI 07-III-04 133.5-134.0 cm	3.46	3.87	23.7
CHI 07-III-04 140.5-141.0 cm	3.23	3.99	25.3
CHI 07-III-04 153.0-153.5 cm	3.06	4.07	26.4
CHI 07-III-04 154.0-154.5 cm	3.26	4.70	28.4
CHI 07-III-04 166.0-166.5 cm	2.59	3.85	27.6
Mean			**25.9**
1σ			**1.7**

Table S8:

Steady-state parameters for Monte Carlo simulations. See text for details of parameters.

Category	Parameter	Units	Values [Range]
Lake Evaporation	Lake Temperature	°C	[22 28]
	w	-	[0.5 0.6]
	V_{eq}	-	[0.6 0.7]
	Xe	-	[0.8 0.9]
	Vapour Temperature	°C	25
	θ_{eq}	-	0.529
	θ_{kin}	-	0.518
Precipitation	$\delta^{18}O$	(per mil, VSMOW)	[-5 -4]
	d-excess		[5 15]
	^{17}Oexcess		[-7 12]

Table S9:

Monte Carlo modeling solutions. *n* defines number of successful simulations.

Data Input					Assumed Freshwater input			Modeled Lakewater			Derived Parameters			RH Uncertainty		Lakewater Uncertainty				
Age (years C.E.)	$\delta^{18}O$	δD	d-excess	^{17}O-excess	Mean $\delta^{18}O$	Mean δD	Mean ^{17}O-ex	Mean $\delta^{18}O$	Mean δD	Mean ^{17}O-ex	Mean RH	Mean T	Mean Xe	min RH	Max RH	min d-excess	Max d-excess	Min ^{17}O-ex	Max ^{17}O-ex	n
Modern	2.98	13.34	-10.47	-20	-4.35	-22.02	7	2.98	13.34	-21	0.80	24.4	0.85	0.76	0.85	-11.44	-9.56	-26	-14	3338
Modern	2.70	10.39	-11.19	-25	-4.45	-23.58	2	2.70	10.38	-25	0.81	24.8	0.85	0.75	0.86	-12.15	-10.30	-31	-19	5379
Modern	2.76	11.18	-10.87	-29	-4.46	-23.14	-1	2.76	11.16	-29	0.80	24.7	0.85	0.75	0.86	-11.84	-9.98	-35	-23	4305
Modern	3.41	13.08	-14.20	-41	-4.53	-22.95	-4	3.42	13.06	-39	0.76	24.8	0.85	0.71	0.81	-15.12	-13.30	-45	-35	2019
Modern	3.42	14.71	-12.68	-31	-4.37	-21.95	1	3.42	14.69	-31	0.78	24.3	0.85	0.73	0.83	-13.59	-11.72	-37	-25	3476
Modern	3.49	15.00	-12.69	-26	-4.35	-21.90	6	3.49	15.00	-26	0.77	24.3	0.85	0.72	0.83	-13.84	-12.00	-32	-20	3373
Modern	3.44	14.46	-13.08	-30	-4.38	-22.14	2	3.44	14.45	-30	0.77	24.5	0.85	0.72	0.83	-13.99	-12.13	-36	-24	3770
Modern	3.43	14.88	-12.56	-35	-4.39	-21.76	-2	3.43	14.86	-35	0.77	24.3	0.85	0.73	0.83	-13.48	-11.65	-41	-29	2828
Modern	3.38	14.50	-12.52	-29	-4.37	-21.99	3	3.38	14.49	-29	0.78	24.4	0.85	0.73	0.83	-13.48	-11.61	-35	-23	3596
Modern	3.41	14.68	-12.57	-27	-4.37	-21.95	5	3.41	14.67	-27	0.78	24.4	0.85	0.73	0.83	-13.53	-11.70	-33	-21	3432
Modern	3.39	14.56	-12.55	-38	-4.43	-21.91	-4	3.40	14.53	-37	0.77	24.4	0.85	0.73	0.82	-13.49	-11.64	-42	-32	2075
Modern	3.40	14.38	-12.83	-25	-4.37	-22.13	6	3.40	14.37	-25	0.78	24.5	0.85	0.73	0.83	-13.75	-11.89	-31	-19	3489
Modern	3.40	14.34	-12.86	-20	-4.31	-22.27	9	3.40	14.33	-22	0.78	24.4	0.85	0.73	0.83	-13.79	-11.93	-26	-15	2018
Modern	3.36	14.27	-12.65	-30	-4.38	-22.09	2	3.36	14.26	-30	0.78	24.5	0.85	0.73	0.83	-13.54	-11.68	-36	-24	3813
Modern	3.68	15.31	-14.18	-40	-4.43	-21.98	-4	3.69	15.29	-39	0.76	24.5	0.85	0.71	0.81	-15.06	-13.23	-45	-34	2368
Modern	2.98	11.98	-11.28	-31	-4.45	-22.97	-1	2.98	11.98	-31	0.79	24.7	0.85	0.74	0.85	-12.79	-10.93	-37	-25	4283
Modern	2.92	11.94	-10.75	-24	-4.41	-22.93	4	2.92	11.93	-24	0.80	24.6	0.85	0.75	0.85	-12.35	-10.49	-30	-18	4700
Modern	2.88	11.63	-10.81	-24	-4.42	-23.10	4	2.88	11.63	-24	0.80	24.6	0.85	0.75	0.85	-12.35	-10.48	-30	-18	4805
Modern	2.69	10.18	-11.36	-32	-4.52	-23.62	-3	2.69	10.17	-31	0.80	24.9	0.85	0.75	0.85	-12.27	-10.41	-38	-26	3635
Modern	2.62	9.59	-11.37	-27	-4.48	-24.06	0	2.62	9.59	-27	0.81	24.8	0.85	0.75	0.87	-12.31	-10.44	-33	-21	5323
Modern	2.88	11.49	-11.52	-23	-4.42	-23.21	5	2.88	11.49	-23	0.80	24.6	0.85	0.75	0.85	-12.46	-10.62	-29	-17	4742
Modern	2.85	11.47	-11.36	-26	-4.43	-23.13	2	2.85	11.46	-26	0.80	24.6	0.85	0.75	0.86	-12.26	-10.39	-32	-20	4745
Modern	2.90	11.61	-11.55	-24	-4.42	-23.17	4	2.90	11.61	-24	0.80	24.6	0.85	0.75	0.85	-12.51	-10.66	-30	-18	4837
Modern	2.91	11.54	-11.74	-33	-4.49	-23.11	-3	2.91	11.53	-32	0.79	24.8	0.85	0.74	0.85	-12.68	-10.81	-39	-27	3656
Modern	2.65	10.02	-11.19	-25	-4.46	-23.82	2	2.65	10.02	-25	0.81	24.8	0.85	0.75	0.86	-12.10	-10.26	-31	-19	5425
Modern	2.79	11.39	-10.93	-33	-4.49	-22.94	-3	2.80	11.37	-32	0.80	24.7	0.85	0.75	0.85	-11.86	-10.01	-39	-27	3062
Modern	3.82	17.21	-13.37	-42	-4.37	-21.01	-5	3.83	17.17	-40	0.76	23.9	0.85	0.71	0.80	-14.26	-12.50	-44	-36	903
Modern	3.13	13.05	-12.96	-36	-4.47	-22.45	-4	3.13	13.03	-35	0.78	24.6	0.85	0.73	0.83	-12.92	-11.07	-41	-30	2617
Modern	3.27	13.69	-12.48	-36	-4.44	-22.29	-3	3.27	13.68	-35	0.78	24.5	0.85	0.73	0.83	-13.40	-11.54	-41	-30	2902
Modern	2.50	9.92	-10.10	-28	-4.48	-23.43	-2	2.50	9.92	-28	0.81	24.8	0.85	0.76	0.87	-10.99	-9.16	-34	-22	4495
Modern	2.62	10.33	-10.87	-31	-4.50	-23.35	-3	2.62	10.32	-30	0.81	24.8	0.85	0.75	0.85	-11.55	-9.70	-37	-25	3618
Modern	3.41	14.30	-12.95	-36	-4.42	-22.17	-3	3.41	14.29	-35	0.77	24.5	0.85	0.72	0.83	-13.91	-12.06	-42	-30	3113
1040.10	4.33	16.97	-17.68	-46	-4.44	-22.19	-4	4.34	16.95	-44	0.72	24.5	0.85	0.67	0.79	-18.58	-16.74	-51	-40	2473
1032.30	3.85	15.01	-15.82	-38	-4.43	-22.66	-1	3.86	15.00	-38	0.75	24.6	0.85	0.69	0.80	-16.76	-14.91	-44	-32	4148
1019.90	3.60	13.70	-15.13	-33	-4.43	-23.12	1	3.61	13.69	-33	0.76	24.6	0.85	0.70	0.82	-16.04	-14.21	-39	-28	4896
1015.30	3.99	15.02	-16.89	-31	-4.40	-23.00	6	3.99	15.01	-31	0.74	24.6	0.85	0.68	0.80	-17.82	-15.96	-37	-25	4586
1006.00	4.57	18.31	-18.22	-35	-4.35	-21.82	6	4.57	18.28	-35	0.72	24.3	0.85	0.66	0.77	-19.14	-17.29	-41	-29	3295
1001.40	4.37	16.48	-18.47		-4.41	-22.73	3	4.37	16.47	-38	0.72	24.5	0.85	0.65	0.79	-19.41	-17.53	-53	-19	11064
996.80	3.65	15.71	-13.50	-30	-4.36	-21.79	4	3.65	15.69	-30	0.77	24.2	0.85	0.71	0.82	-14.41	-12.56	-36	-24	3296
992.20	3.87	15.18	-15.78	-34	-4.40	-22.59	2	3.87	15.17	-34	0.75	24.5	0.85	0.69	0.81	-16.71	-14.85	-40	-28	4563
987.60	4.37	16.63	-18.34	-31	-4.37	-22.60	8	4.37	16.62	-32	0.72	24.5	0.85	0.66	0.78	-19.27	-17.40	-37	-26	3557
973.10	3.98	15.87	-15.94	-36	-4.40	-22.28	1	3.98	15.86	-36	0.75	24.4	0.85	0.69	0.80	-16.86	-15.02	-42	-31	3969
962.40	4.17	17.00	-16.37	-31	-4.35	-21.89	6	4.17	16.99	-32	0.74	24.4	0.85	0.68	0.79	-17.29	-15.44	-37	-25	3437
951.60	4.24	16.41	-17.48	-36	-4.40	-22.50	3	4.24	16.41	-36	0.73	24.5	0.85	0.67	0.79	-18.41	-16.55	-42	-30	4427
946.30	3.87	15.46	-15.49	-42	-4.46	-22.30	-4	3.87	15.44	-41	0.75	24.5	0.85	0.69	0.80	-16.41	-14.58	-47	-36	2401
930.20	3.73	15.41	-14.46	-40	-4.43	-22.05	-3	3.74	15.39	-39	0.76	24.5	0.85	0.70	0.81	-15.39	-13.53	-45	-34	2637
924.90	3.98	16.35	-15.48	-47	-4.49	-21.91	-5	3.99	16.31	-44	0.74	24.3	0.85	0.69	0.78	-16.35	-14.57	-48	-41	694
919.50	3.84	15.56	-15.13	-32	-4.38	-22.23	3	3.84	15.55	-32	0.75	24.4	0.85	0.70	0.81	-16.07	-14.20	-38	-26	4018
903.10	4.85	18.38	-20.42	-36	-4.37	-22.44	7	4.85	18.38	-36	0.70	24.4	0.85	0.63	0.76	-21.36	-19.49	-42	-30	3638
835.30	4.07	16.44	-16.10	-33	-4.37	-22.07	4	4.07	16.43	-33	0.74	24.4	0.85	0.68	0.80	-17.03	-15.17	-39	-28	3741
823.70	4.18	15.88	-17.52	-43	-4.44	-22.64	-3	4.18	15.87	-42	0.73	24.6	0.85	0.67	0.79	-18.45	-16.62	-48	-37	3760
812.10	4.56	17.72	-18.77	-36	-4.38	-22.22	5	4.56	17.71	-36	0.72	24.4	0.85	0.65	0.77	-19.71	-17.85	-42	-30	3969
800.40	4.42	17.01	-18.33	-36	-4.39	-22.46	4	4.42	16.99	-36	0.72	24.5	0.85	0.66	0.78	-19.26	-17.39	-42	-30	4324
794.50	4.77	18.25	-19.89	-43	-4.38	-22.21	0	4.77	18.23	-43	0.70	24.4	0.85	0.64	0.76	-20.82	-18.96	-49	-37	4039
776.90	3.69	15.91	-13.62	-33	-4.35	-21.70	1	3.69	15.90	-33	0.76	24.2	0.85	0.70	0.82	-14.56	-12.70	-39	-27	3277
771.00	4.26	17.30	-16.80	-32	-4.35	-21.91	6	4.26	17.28	-32	0.73	24.3	0.85	0.68	0.79	-17.74	-15.88	-38	-26	3378
765.20	4.70	18.78	-18.81	-35	-4.34	-21.74	6	4.70	18.77	-35	0.71	24.3	0.85	0.64	0.77	-19.74	-17.89	-41	-29	3206
759.30	4.12	15.92	-17.07	-33	-4.40	-22.61	5	4.13	15.91	-33	0.74	24.5	0.85	0.68	0.79	-18.01	-16.15	-39	-27	4217
759.30	4.37	16.61	-18.31	-32	-4.37	-22.61	7	4.37	16.61	-32	0.72	24.5	0.85	0.66	0.78	-19.24	-17.37	-37	-26	3658
753.40	4.42	16.86	-18.46	-45	-4.44	-22.46	-3	4.42	16.85	-44	0.72	24.6	0.85	0.66	0.77	-19.40	-17.56	-51	-39	3330
747.40	4.01	16.17	-15.88	-45	-4.47	-22.08	-5	4.01	16.13	-43	0.74	24.4	0.85	0.69	0.78	-16.81	-14.97	-48	-40	1354
741.50	4.34	16.14	-18.57	-48	-4.51	-22.80	-4	4.34	16.12	-46	0.72	24.7	0.85	0.66	0.77	-19.49	-17.64	-52	-42	2273
634.30	3.85	15.11	-15.67	-26	-4.35	-22.70	8	3.85	15.11	-27	0.75	24.4	0.85	0.69	0.81	-16.58	-14.73	-32	-20	3045
625.30	4.46	17.73	-17.93	-43	-4.39	-21.92	-2	4.46	17.71	-43	0.72	24.4	0.85	0.66	0.78	-18.86	-17.01	-49	-37	3296
620.70	3.86	15.00	-15.91	-19	-4.21	-23.35	10	3.86	15.00	-22	0.77	24.0	0.85	0.72	0.81	-16.74	-15.05	-25	-17	461

Table S10:

Output table of Bayesian age-depth analysis. Mean ages display single ‘best’ model based on the weighted mean age for each depth. Positive and negative age errors represent 95% confidence intervals.

Depth (cm)	Mean Age (C.E.)	Positive Age Error (C.E.)	Negative Age Error (C.E.)
0	2004.4	2025.6	1953.5
1	2000.8	2021.3	1948.7
2	1993.6	2019.6	1938.9
3	1986.5	2018.6	1920.1
4	1979.7	2018.5	1897.6
5	1972.9	2018.7	1874.6
6	1965.4	2014.2	1867.4
7	1958	2011.8	1859.3
8	1950.5	2010	1846.3
9	1943	2008.4	1831.4
10	1935.6	2006.6	1814
11	1928.4	2001.4	1805.9
12	1921	1997.7	1796.8
13	1913.7	1995.4	1787.2
14	1906.5	1993.2	1773.1
15	1899.2	1991.6	1758.2
16	1891.9	1985.5	1751.1
17	1884.4	1981.2	1744
18	1877.2	1978	1731.8
19	1869.9	1975.3	1719
20	1862.8	1973.4	1705
21	1855.6	1967.1	1698.7
22	1848.4	1961.7	1692.4
23	1841.2	1957.2	1684.3
24	1833.9	1953.8	1673.3
25	1826.7	1950.8	1661.2
26	1819.5	1942.6	1654.2
27	1812.4	1937.1	1648.5
28	1805.3	1932.8	1640.3
29	1798.2	1928.9	1630.3
30	1791.1	1925.5	1619.9
31	1783.7	1917.6	1612.2
32	1776.4	1911.4	1605
33	1769.1	1907.3	1597.2
34	1761.7	1902.1	1588.6
35	1754.3	1899.1	1576.3
36	1747.2	1889.9	1569.6
37	1740	1884.8	1562.5
38	1732.8	1878.6	1555.9
39	1725.6	1874.2	1546.3
40	1718.4	1870.9	1535.3
41	1711.1	1863.1	1530
42	1703.8	1856.5	1524.1
43	1696.5	1851	1515.5
44	1689.3	1846.6	1506.5
45	1682	1843	1499.4
46	1674.9	1836	1494.1
47	1667.6	1829.3	1488
48	1660.4	1824.2	1480.7
49	1653.1	1820	1471.6
50	1646	1817.4	1463.2
51	1638.8	1808.4	1457.4
52	1631.7	1801.1	1450.9
53	1624.5	1794.7	1443.7
54	1617.5	1788.8	1433.9
55	1610.6	1783.3	1424
56	1603.3	1774.4	1418.9
57	1596	1767.7	1411.9
58	1588.7	1761.3	1404.7
59	1581.3	1756.1	1395.4
60	1574.3	1752.8	1386.9
61	1567	1742.5	1382.3
62	1559.7	1735.3	1377.7
63	1552.4	1730	1370.6
64	1544.9	1722.8	1363.1
65	1537.5	1716.8	1353.5
66	1530.2	1706.5	1349.3
67	1522.8	1698.3	1344.9
68	1515.2	1692.2	1338.1
69	1507.7	1687.9	1331.8
70	1500.3	1683	1323.9
71	1493.2	1671.5	1319.3
72	1486.2	1664.5	1313.4
73	1479.2	1658	1305.6
74	1472	1653.6	1297.6
75	1465	1648.5	1290.1
76	1457.7	1638.8	1285.7
77	1450.5	1631.8	1280.5
78	1443.2	1625.4	1273.7
79	1435.9	1620.4	1267.4
80	1428.6	1614	1258.6
81	1421.8	1604.9	1253.8
82	1415.1	1595.6	1248.3
83	1408.2	1588.2	1241.6
84	1401.5	1581.9	1234.6
85	1394.6	1576.8	1225.3
86	1387.7	1567.5	1221.4
87	1380.6	1557.7	1216.6

Table S10 Continued:

Depth (cm)	Mean Age (C.E.)	Positive Age Error (C.E.)	Negative Age Error (C.E.)
88	1373.7	1549.7	1211.5
89	1366.7	1543	1204.8
90	1359.8	1537.7	1195.6
91	1352.9	1529.9	1191.4
92	1345.8	1522	1186.4
93	1338.8	1517.1	1180.5
94	1331.8	1510.2	1174.9
95	1324.8	1505	1167.6
96	1317.7	1494.9	1164
97	1310.6	1483.8	1159.3
98	1303.4	1476.3	1153.2
99	1296.2	1469.1	1146.4
100	1288.9	1464.9	1138.6
101	1281.8	1452.1	1135.1
102	1274.5	1440.8	1130.8
103	1267.4	1432.4	1124.8
104	1260.1	1426.3	1118.1
105	1252.9	1419.7	1110.5
106	1245.3	1407.6	1107.3
107	1237.8	1397.7	1103.1
108	1230.2	1389.7	1098.2
109	1222.7	1383.5	1092.9
110	1215.1	1376.9	1085.2
111	1208.3	1365.3	1082.2
112	1201.6	1354.9	1078.7
113	1194.9	1345.4	1074.8
114	1188.2	1337	1070.4
115	1181.5	1329.3	1064.3
116	1174.6	1318.1	1061.3
117	1167.8	1308.8	1058.7
118	1160.8	1300.9	1055.5
119	1154	1293.2	1050.4
120	1147	1288.3	1044
121	1140.1	1274.1	1042.7
122	1133.3	1262.6	1040.7
123	1126.3	1252.7	1038
124	1119.2	1244.4	1034.8
125	1112.2	1237.9	1029
126	1105.6	1224.3	1027.2
127	1098.6	1211.8	1025.1
128	1091.7	1203	1021.4
129	1084.8	1195.7	1016.6
130	1078.1	1190.9	1010.3
131	1068.7	1175.8	1005.6
132	1059.4	1165.4	997.3
133	1050.2	1157.9	985
134	1041	1151.4	967.4
135	1032.2	1146.8	948
136	1019.3	1127.1	940.2
137	1006.2	1110.5	925.7
138	992.9	1099.2	902.2
139	979.7	1092	874.6
140	966.9	1087	847.5
141	953.1	1056.6	838.5
142	939.1	1029.7	828.4
143	925	1011.1	814.5
144	911.1	997.8	795.5
145	897.2	989.4	770.4
146	881.1	965.8	761
147	865	954.1	749.2
148	848.9	946	733.4
149	832.9	940.7	710.8
150	817	936.9	681
151	801	915.2	676.2
152	784.7	901.2	670.8
153	768.4	891.6	663.9
154	752.2	882.9	654.6
155	736.1	876.9	636.7
156	720.2	835.6	635.2
157	704.1	800.2	632.2
158	687.7	772.6	628.7
159	671.2	753.8	622.7
160	654.8	741.2	610
161	647	729.3	605.5
162	639.3	722.7	597.6
163	631.9	717.3	586.6
164	624.3	712.6	573.6
165	616.7	706.5	557.8
166	610.7	695.1	552.1
167	604.5	685.3	543.5
168	598.5	676.1	531.9
169	592.4	668.6	517.4
170	586.5	664.3	501
171	579.4	652.7	493.8
172	572.3	644.9	485.1
173	565.4	636.9	475.4
174	558.6	632.7	462.1
175	551.8	629.9	446.8

Table S10 Continued:

Depth (cm)	Mean Age (C.E.)	Positive Age Error (C.E.)	Negative Age Error (C.E.)
176	543.2	620.8	439.9
177	534.4	614.5	432.8
178	525.5	610	421.9
179	516.8	605.7	408.1
180	508.2	602.3	393.1
181	499.2	591.9	386.2
182	490.1	584	379.1
183	481.2	577.8	372
184	472.3	573.4	359.3
185	463.6	569.9	345.3
186	453	556.8	339.1
187	442.5	547.3	333.1
188	432	541.6	321.9
189	421.3	535.7	307.6
190	410.7	531.3	291.9
191	397.5	510.2	284.1
192	384.3	497.5	274.8
193	371.1	487.3	260.9
194	357.9	480.5	243.4
195	344.7	474.6	220.4
196	331.6	445.6	214.7
197	318.4	418.9	207.4
198	305.3	400.5	198.4
199	292.3	387.3	187.3
200	279.3	377.2	170.3
201	269.7	362.3	165.8
202	260	351.9	158.6
203	250.1	344	148.5
204	240.1	338.9	133.1
205	230.2	334.5	116.1
206	222	325.9	110.1
207	213.7	318.2	101.8
208	205.4	312.6	92.2
209	197.3	308.2	81.8
210	189.2	304.2	67.6
211	180.9	292.6	61.5
212	172.5	284.1	54.1
213	164.3	277.8	44.4
214	155.9	273.3	33.5
215	147.7	269.3	21.1
216	138.5	258.6	13.7
217	129.4	250.6	4.4
218	120.3	243.8	-8.6
219	111.1	239	-23.7
220	102.2	233	-42.4
221	92.1	223.8	-52.3
222	82.2	216.4	-67
223	72.5	210.5	-82.4
224	62.7	206	-101.8
225	52.9	202.7	-127.1
226	42.9	192.2	-136.3
227	32.8	185.8	-147
228	22.8	179.4	-160.1
229	12.7	174.2	-176
230	2.6	169.9	-196.4
231	-7.1	160.7	-207.1
232	-16.7	153.4	-217
233	-26.6	145.9	-228.7
234	-36.3	141	-243.2
235	-45.6	136.8	-264.2
236	-55.4	126.2	-271.6
237	-65.1	116.9	-281.5
238	-74.8	108.7	-292
239	-84.6	103	-306.6
240	-94.4	97	-322.6
241	-104.1	87.4	-328.6
242	-114	79.5	-336.7
243	-123.8	72.5	-347.8
244	-133.5	66.9	-362.9
245	-143.2	61.6	-378.6
246	-153.5	51	-388.6
247	-163.6	41.9	-396.6
248	-173.9	33.9	-407.9
249	-184.3	25.8	-420.7
250	-194.4	21.2	-436.8
251	-204.6	8.8	-446.1
252	-214.8	-1.1	-455.2
253	-224.9	-7.4	-465.3
254	-235	-13.6	-475.6
255	-244.9	-20.1	-491.8
256	-254.8	-30.3	-498.6
257	-264.7	-39.7	-507.6
258	-274.6	-47.6	-516.9
259	-284.8	-55.1	-528.2
260	-294.6	-62	-541.2

Supplementary Figures:

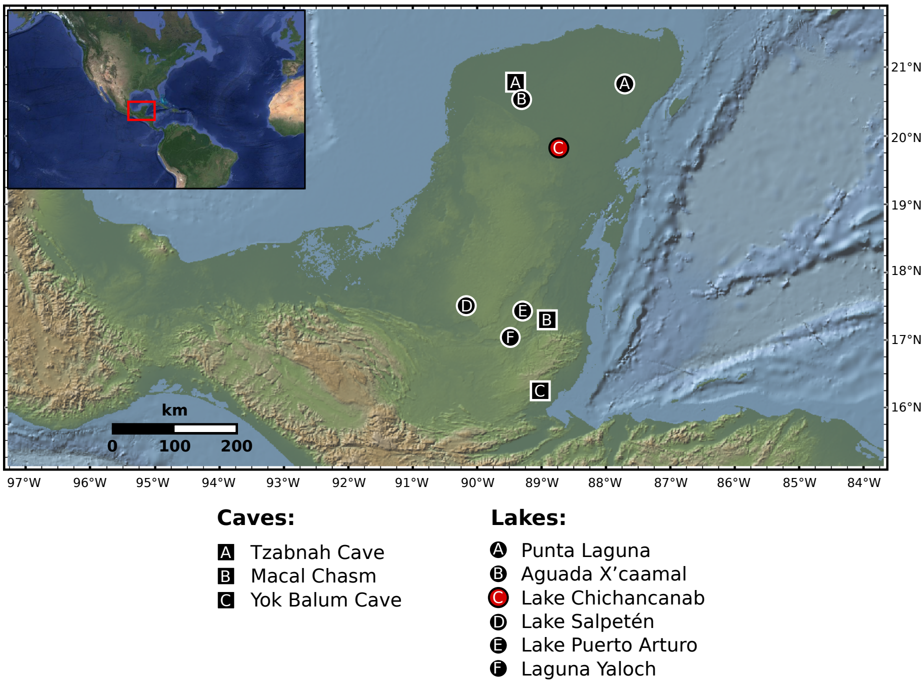

Fig. S1: Map of the Maya Lowlands displaying the locations of proxy climate archives (north to south); the Chaac speleothem of Tzabnah Cave (*6*); Punta Laguna (*4*); Aguada X'caamal (*52)*; Lake Chichancanab (this study) (*1-3*); Lake Puerto Arturo (*53*); Laguna Yaloch (*8*); Macal Chasm (*54*); Lake Salpetén (*9*); the Yok I speleothem of Yok Balum Cave (*7*).

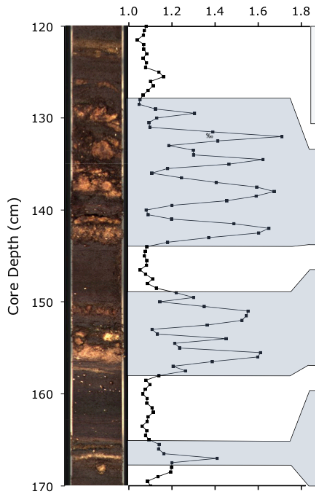

$\delta^{18}O$ (‰)	$\delta^{17}O$ (‰)	δD (‰)	^{17}O-excess (per meg)	d-excess (‰)	Age lower bound (± error)	Age upper bound (± error)
3.1 ± 0.4	1.6 ± 0.2	12.7 ± 1.9	-28 ± 7	-11.8 ± 1.1	1994 ± 0	2010 ± 0
4.1 ± 0.3	2.1 ± 0.2	16.1 ± 1.2	-36 ± 5	-16.5 ± 1.7	939 ± 100	1092 ± 90
4.3 ± 0.3	2.2 ± 0.2	16.9 ± 0.9	-38 ± 6	-17.6 ± 1.7	720 ± 100	849 ± 106
4.1 ± 0.4	2.1 ± 0.2	16.0 ± 1.6	-29 ± 12	-16.5 ± 1.2	602 ± 71	611 ± 72

Fig. S2: (**Left**) Image of split core CH1 7-III-04 (*3*). Sediments are composed of interbedded gypsum- and organic-rich strata containing abundant shell material. Solid black line represents the GRA bulk density record measured on core CH1 7-III-04 (*3*). Periods of gypsum precipitation are indicated by positive density excursions >1.2 g/cm^3. (**Right**) The $\delta^{18}O$, $\delta^{17}O$, δD and d-excess (‰, VSMOW) and ^{17}O-excess (per meg, VSMOW) (±1σ) of the modern lake water and measured GHW during each of the three periods of gypsum deposition (after correction for known fractionation factors (*23*) at 26°C) are displayed.

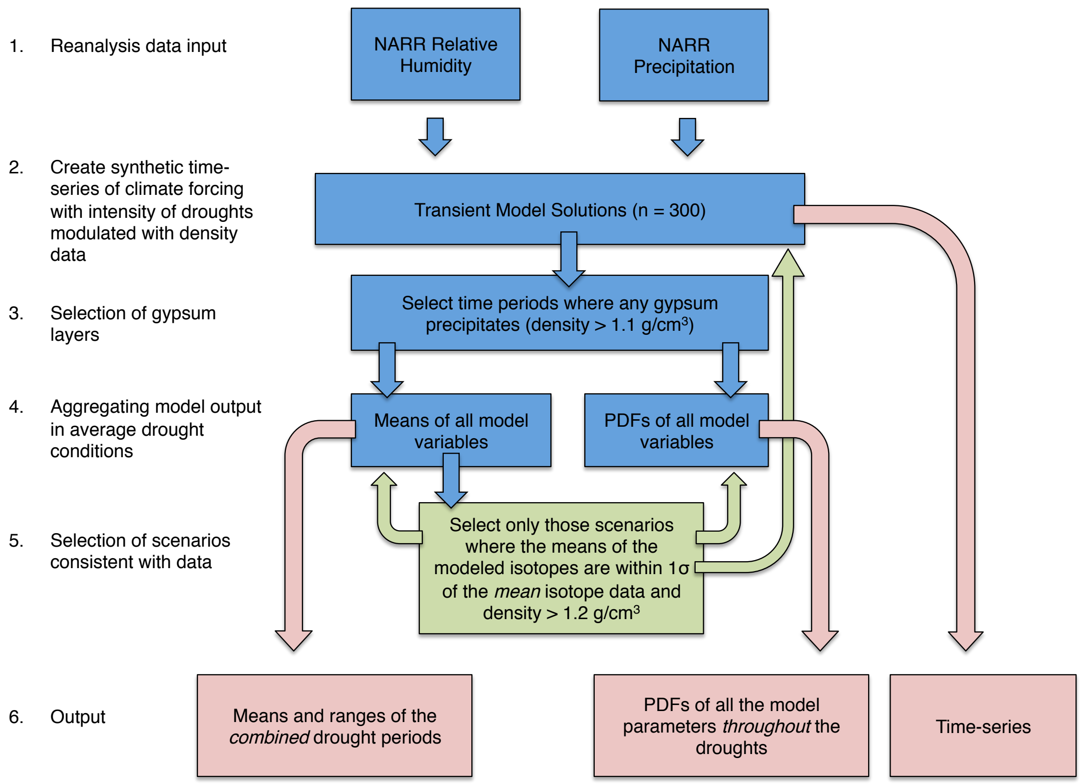

Fig. S3: Transient model summary of forcing (blue boxes and arrows), scenario selection by model/data comparison (green boxes and arrows), and model output (red boxes and arrows).

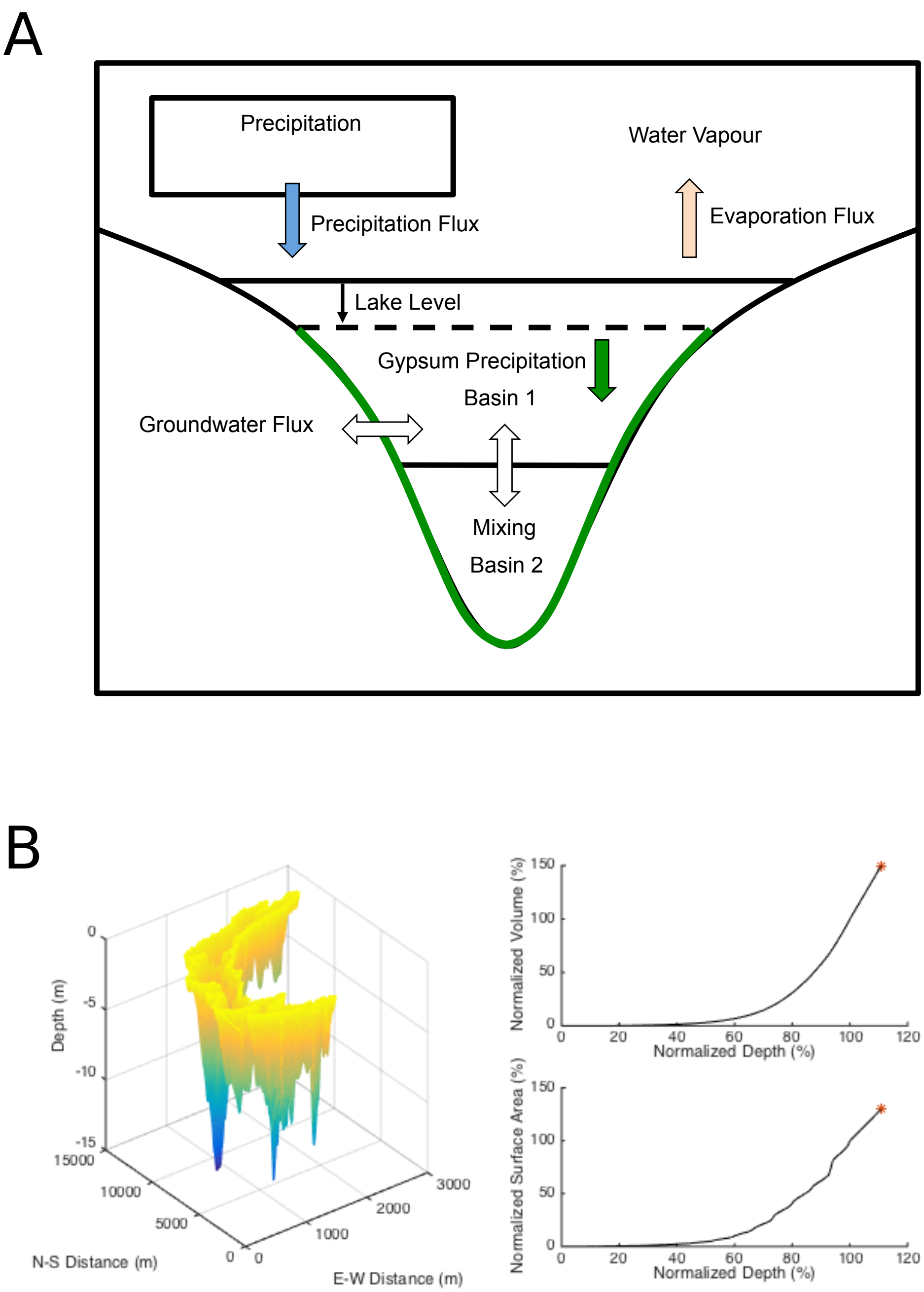

Fig. S4: (**A**) Diagrammatic representation of the two-box model used in transient model scenarios. (**B**) The bathymetry of Lake Chichancanab used in the transient model (*3*), and generated normalized surface area and volume vs normalized depth.

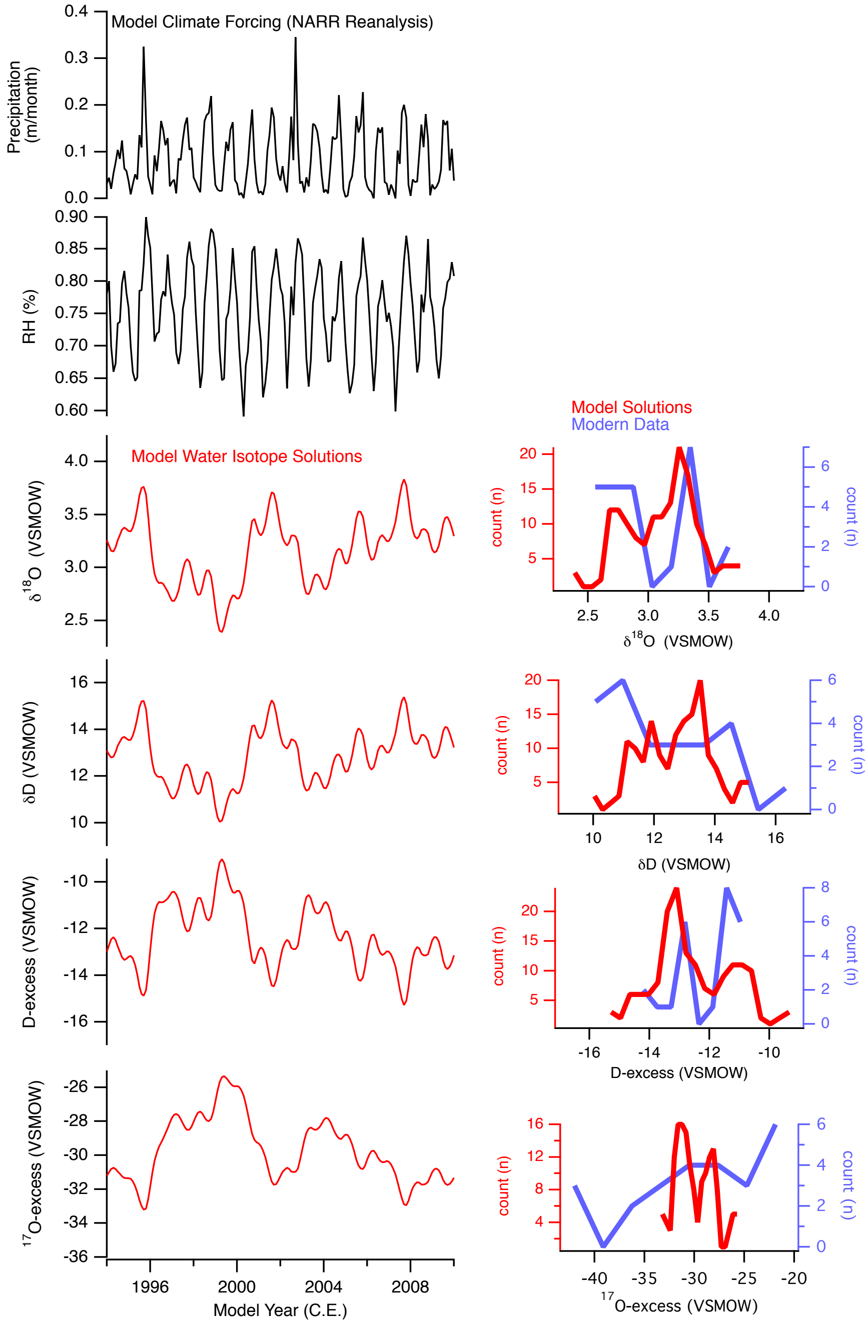

Fig. S5: Transient model climate forcing. The transient model is forced with North American Regional Reanalysis (NARR) data for local precipitation and relative humidity (RH_n) across the modern sampling period from 1994 to 2010 (black lines). Modeled water isotope solutions (red lines) are then compared to measured modern data (blue lines) as histograms (right panel). The model successfully reproduced the mean of modern isotope data, with insignificant gypsum precipitation. The time interval from 1994 to 2010 is subsequently used as the baseline for comparison to paleo-simulations.

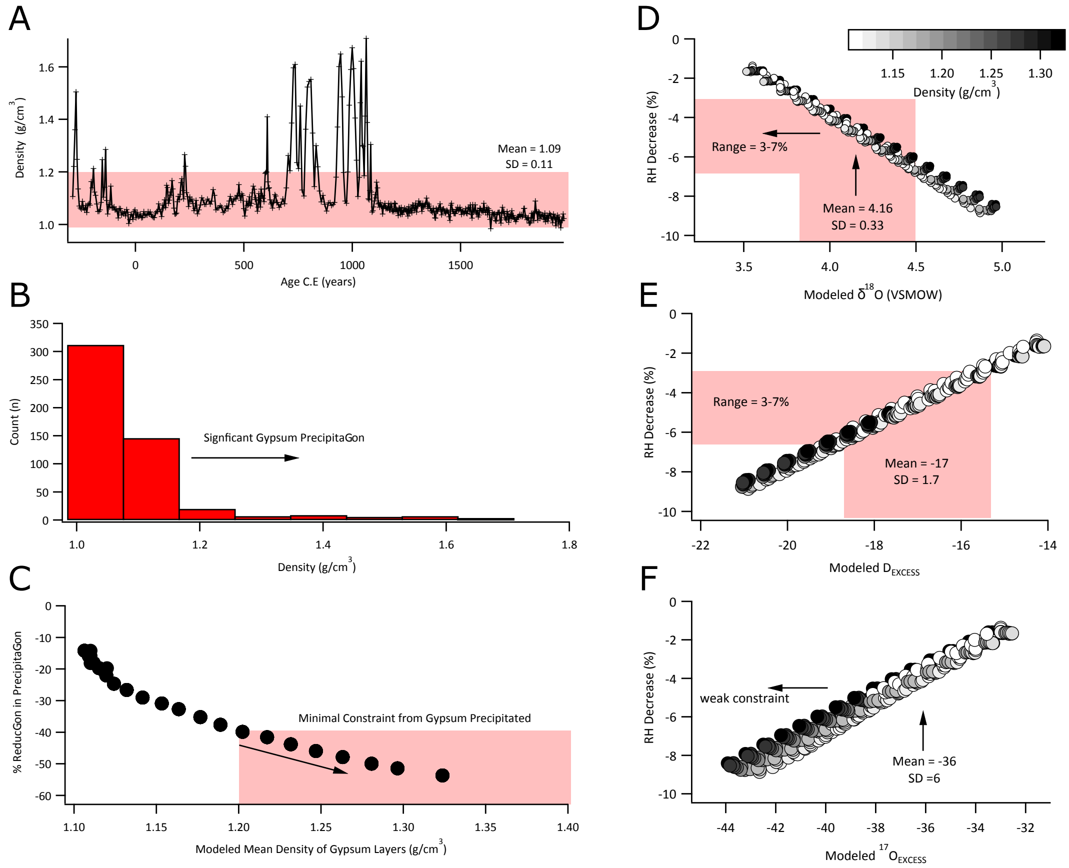

Fig. S6: Transient model precipitation and relative humidity scenarios. (**A**) GRA bulk density record of core CH1 7-III-04 (*3*). From 500 B.C. to 2000 C.E., mean (±1σ) sediment density = 1.09±0.11 g/cm^3 (red horizontal band). (**B**) Histogram of counts from GRA bulk density record from 500 B.C. to 2000 C.E. (**C**) Example of the relationship between modeled mean core density (g/cm^3) and the modeled reduction in precipitation (%). Varying the minimum cut-off point from which modeled data are compared to GHW data changes the baseline precipitation reduction estimate. Example of modeled δ^{18}O (**D**), d-excess (**E**), and ^{17}O-excess (**F**) data plotted as a function of modeled densities. Mean GHW (±1σ) data are then compared to modeled runs to derive %RH$_n$ decrease.

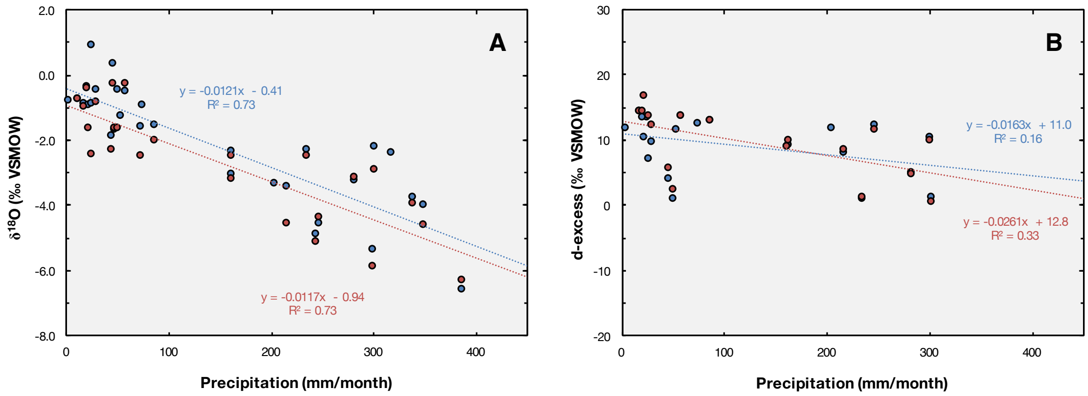

Fig. S7: The amount effect relationship between monthly precipitation amount and monthly mean rainfall (**A**) $\delta^{18}O$ and (**B**) d-excess during the dry (November to May) and rainy seasons (June to October) from the IAEA station in Veracruz, México (years 1969 to 1985) and Hobonil (20°00'59"N 89°01'13"W; 2006 to 2009). Both raw (blue circles) and amount-weighted (red clircles) show that rainfall $\delta^{18}O$ is negatively correlated to the amount of precipitation on seasonal time scales, whereas there is no significant amount effect displayed by d-excess.

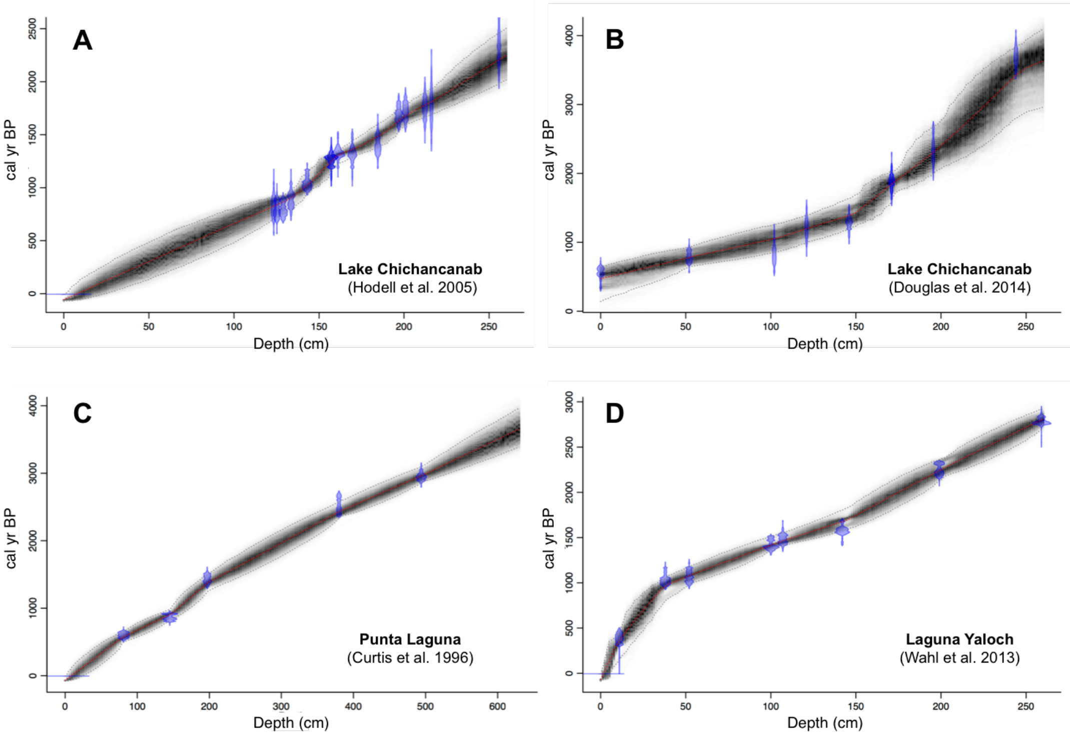

Fig. S8: Bayesian age models produced for (**A**) core CHI 7-III-04 of Lake Chichancanab (*3*), (**B**) Plant waxes of Lake Chichancanab (*50*), (**C**) Punta Laguna (*4*) and (**D**) Laguna Yaloch (*8*) by the program BACON (*49*). Dark shading indicates more likely calendar ages at each depth and the red lines indicate the best-fit age model.

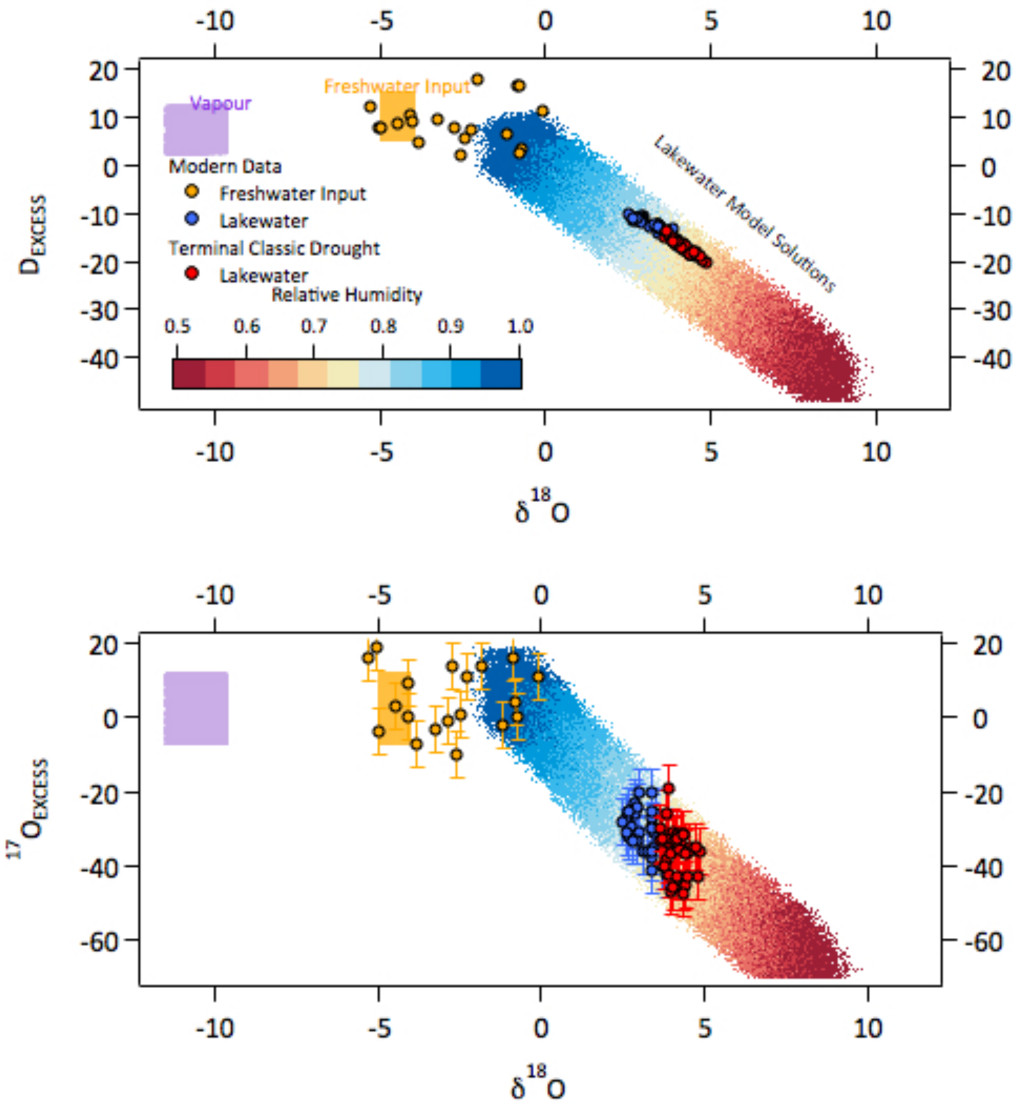

Fig. S9: Monte Carlo Modeling Scenarios in which the isotopic composition of the paleo-lake water (red markers) and modern waters (blue markers) is shown in a cross plot of δ^{18}O–d-excess (upper panel) and δ^{18}O-^{17}O-excess (lower panel). Modern freshwater data are shown (yellow markers). With the data, a suite of model solutions are plotted with the assumed freshwater input range (yellow box), atmospheric water vapor range (purple box) and the complete range of model solutions for the isotopic composition of the lake with the marker coloring representing the range in normalized relative humidity.

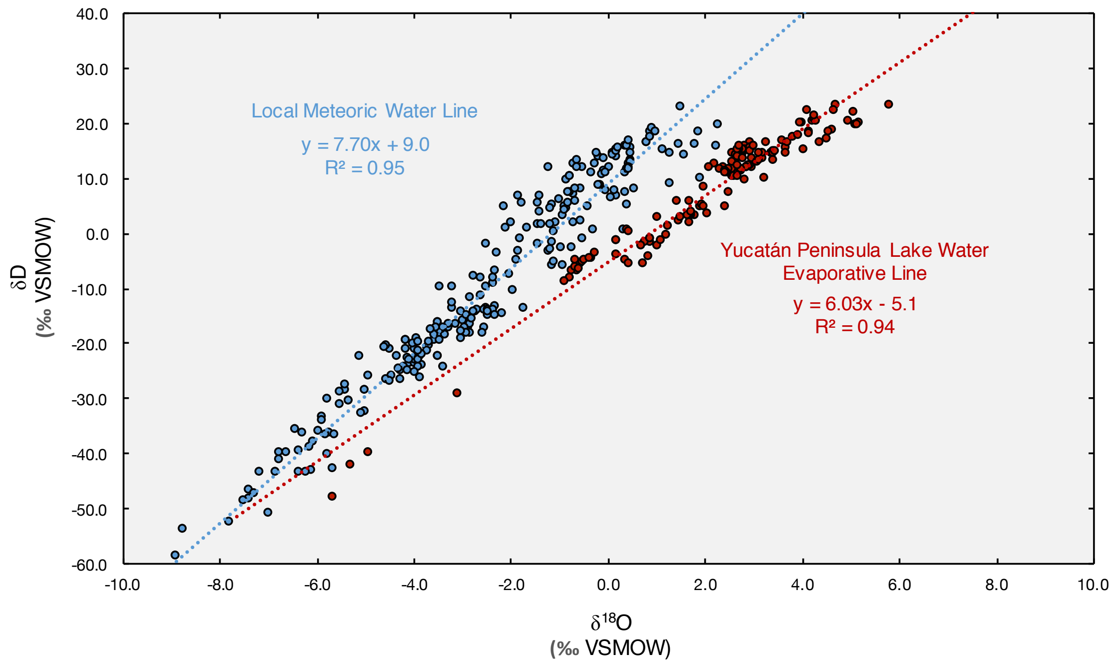

Fig. S10: $\delta^{18}O$ and δD of rain, surface water, and ground water (blue circles). Dashed blue line represents the local meteoric water line estimated by least-squares linear regression through rain, surface and groundwater data. Red circles indicate measurements made on lakes with varying hydrologic budgets and evaporative losses across the Yucatán Peninsula. Dashed red line represents the evaporative line (with slope = 6.0) estimated by least-squares linear regression using lake data. Note that this slope is comparable to the slope of modern data from Lake Chichancanab alone (slope = 5.1), and is significantly different from that of the slope of measured GHW data (slope = 3.1) (Fig. 2).

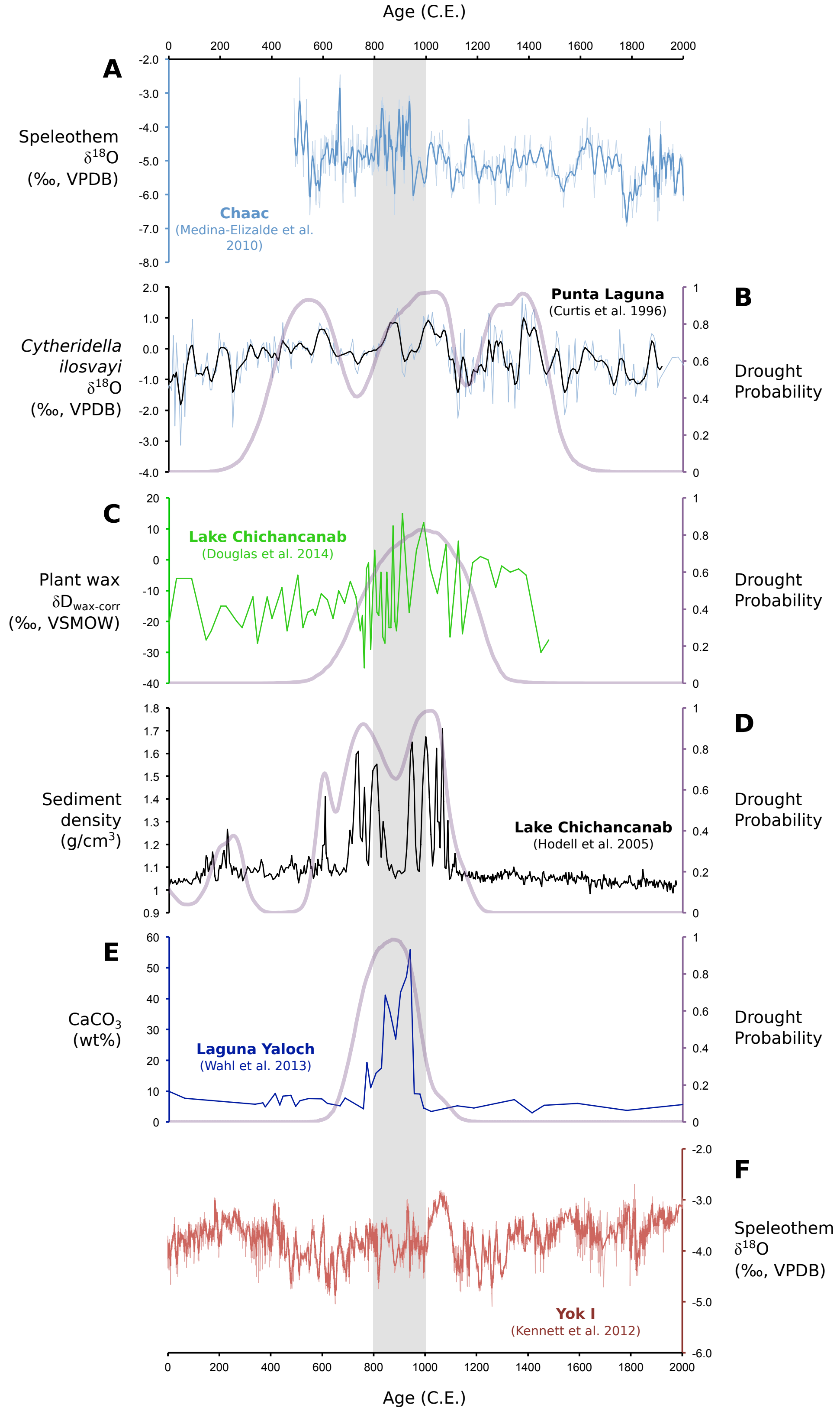

Fig. S11: Selection of palaeoclimate records from the Maya Lowlands, arranged from north to south: (**A**) Chaac speleothem (Tzabnah Cave) $\delta^{18}O$ (*6*); (**B**) Punta Laguna

$\delta^{18}O$ (*4*); (**C**) Lake Chichancanab $\delta D_{wax\text{-}corr}$ (*50*); (**D**) Lake Chichancanab sediment density (*3*) (**E**) Laguna Yaloch weight percent calcium carbonate ($CaCO_3$) (*8*); (**F**) Yok I speleothem (Yok Balum Cave) $\delta^{18}O$ (*7*). Age uncertainty analysis for proxy sites displays "drought probabilities" in given time intervals for the proxy data. All age models were calculated using Bayesian age analyses (Fig. S8). The vertical gray bar indicates the TCP between 800 and 1000 C.E. $\delta D_{wax\text{-}corr}$ values indicate δD_{wax} values corrected for the influence of vegetation change (*50*). **Abbreviation**: VPDB, Vienna Pee Dee Belemnite; VSMOW, Vienna Standard Mean Ocean Water.

Supplementary References:

[31] E. Playa, C. Recio, J. Mitchell. Extraction of gypsum hydration water for oxygen isotopic analysis by the guanidine hydrochloride reaction method. *Chem. Geol.* **217**(1), 89-96 (2005).

[32] E. J. Steig, V. Gkinis, A. J. Schauer, S. W. Schoenemann, K. Samek, J. Hoffnagle, K. J. Dennis, S. M. Tan. Calibrated high-precision ^{17}O-excess measurements using laser-current tuned cavity ring-down spectroscopy. *Atmos. Meas. Tech.* **7**, 2421–2435 (2014).

[33] S. W. Schoenemann, A. J. Schauer, E. J. Steig. Measurement of SLAP and GISP δ^{17}O and proposed VSMOW-SLAP normalization for ^{17}O-excess. *Rapid Commun. Mass Spec.* **27**, 582–590 (2013).

[34] E. Barkan, B. Luz. Diffusivity fractionations of $H_2{}^{16}O/H_2{}^{17}O$ and $H_2{}^{16}O/H_2{}^{18}O$ in air and their implications for isotope hydrology. *Rapid Commun. Mass Spectrom.* **21**, 2999–3005 (2007).

[35] A. L. Grauel, D. A. Hodell, S. F. Bernasconi. Quantitative estimates of tropical temperature change in lowland Central America during the last 42 ka. *Earth Planet. Sci. Lett*. **438**, 37–46 (2016).

[36] J. Li, M. Li, X. Fang, G. Zhang, W. Zhang, X. Liu. Isotopic composition of gypsum hydration water in deep Core SG-1, western Qaidam basin (NE Tibetan Plateau), implications for paleoclimatic evolution. *Glob. Planet. Change.* **155**, 70–77 (2017).

[37] M. C. Ball, L. S. Norwood. Studies in the system calcium sulphate–water. Part I. Kinetics of dehydration of calcium sulphate dihydrate. Journal of the Chemical Society A: Inorganic, Physical, Theoretical, 1633-1637 (1969).

[38] J. K. Warren. *Evaporites: A geological compendium* (Springer, New York, 2016).

[39] C. Spötl, T. W. Vennemann, Continuous-flow isotope ratio mass spectrometric analysis of carbonate minerals. *Rapid Commun. Mass Spectrom.* **17**, 1004–1006 (2003).

[40] E. Perry, G. Velazquez-Oliman, L. Marin. The hydrogeochemistry of the karst aquifer system of the northern Yucatán Peninsula Mexico. *Int. Geol. Rev*. **44**, 191–221 (2002).

[41] R. E. Criss. *Principles of Stable Isotope Distribution* (Oxford Univ. Press, Oxford, U.K. 1999).

[42] J. Horita, D. J. Wesolowski. Liquid-vapor fractionation of oxygen and hydrogen isotopes of water from the freezing to the critical temperature. G*eochim. Cosmochim. Acta.* **58**, 3425–3437 (1994).

[43] E. Barkan, B. Luz. High precision measurements of $^{17}O/^{16}O$ and $^{18}O/^{16}O$ ratios in H_2O. *Rapid Commun. Mass Spectrom*, **19**(24), 3737-3742 (2005).

[44] J. J. Gibson, S. J. Birks, Y. Yi. Stable isotope mass balance of lakes: a contemporary perspective. *Quat. Sci. Rev.* **131**, 316–328 (2016).

[45] E. L. Grossman, T. Ku. Oxygen and carbon fractionation in biogenic aragonite: temperature effect. *Chem. Geol.* **59**, 59–74 (1986).

[46] R. Uemura, E. Barkan, O. Abe, B. Luz. Triple isotope composition of oxygen in atmospheric water vapor. *Geo. res. let,* **37**(4) (2010).

[47] R. Soler-Bientz, S. Watson, D. Infield. Wind characteristics on the Yucatán Peninsula based on short term data from meteorological stations. *Energy Conversion and Management,* **51**(4), 754-764 (2010).

[48] Z. Sofer, J. R. Gat. The isotope composition of evaporating brines: effect of the isotopic activity ratio in saline solutions. *Earth Planet. Sci. Lett*. **26**, 179–186 (1975).

[49] M. Blaauw, J. A. Christen. Flexible paleoclimate age-depth models using an autoregressive gamma process. *Bayesian Anal.* **6** (3), 457-474 (2011).

[50] P. M. Douglas, M. Pagani, T. I. Eglinton, M. Brenner, D. A. Hodell, J. H. Curtis, K. F. Ma, A. Breckenridge. Pre-aged plant waxes in tropical lake sediments and their influence on the chronology of molecular paleoclimate proxy records. *Geochim. Cosmochim. Acta* **141**, 346–364 (2014).

[51] T. Bhattacharya, J. C. H. Chiang, W. Cheng. Ocean-atmosphere dynamics linked to 800-1050 CE drying in Mesoamerica. *Quatern. Sci. Rev.* **169**, 263-277 (2017).

[52] D. A. Hodell, M. Brenner, J. H. Curtis, R. Medina-Gonzalez, E. I. Can, A. Albornaz-Pat, T. P. Guilderson. Climate change on the Yucatán Peninsula during the Little Ice Age. *Quat. Res.* **63**, 109–21 (2005).

[53] D. Wahl, R. Byrne, L. Anderson. An 8700 year paleoclimate reconstruction from the southern Maya lowlands. *Quat. Sci. Rev.* **103**, 19–25 (2014).

[54] J. W. Webster, G. A. Brook, L. B. Railsback, H. Cheng, R. L. Edwards, C. Alexander, P. P. Reeder. Stalagmite evidence from Belize indicating significant droughts at the time of Preclassic Abandonment, the Maya Hiatus, and the Classic Maya collapse. *Palaeogeogr. Palaeoclimatol. Palaeoecol.* **250**, 1–17 (2007).